Available online at www.sciencedirect.com
SCIENCE DIRECT®
Journal of Sound and Vibration 264 (2003) 795–833
JOURNAL OF SOUND AND VIBRATION
www.elsevier.com/locate/jsvi

Analyses for random flow-induced vibration of cylindrical structures subjected to turbulent axial flow

Ll.R. Curling[1], M.P. Païdoussis*

Department of Mechanical Engineering, McGill University, 817 Sherbrooke Street West, Montreal, Que., Canada H3A 2K6

Received 24 August 2001; accepted 19 July 2002

Abstract

In this paper, stochastic analytical equations for obtaining the vibratory response of bundles of cylinders in turbulent axial flow, with various degrees of computational efficiency, are presented. Lateral components of the turbulent fluid force-per-unit-length cross-spectral densities in a bundle of cylinders are obtained by the integration of differential wall-pressure fluctuations around the circumferences of the cylinders. These quantities are used as excitation in the calculation of random vibration response spectral densities of the cylindrical structures. Properties of symmetry applicable to lateral forces in bundles of symmetrically arranged cylinders are also discussed.

1. Introduction

The calculation of turbulent fluid forces acting on cylindrical structures subjected to axial flow is important to the study of vibration of bundles of fuel rods in nuclear reactor cores and tube banks in heat exchangers.

Previously [1–3], it was shown that the dynamical equations governing the vibratory motions of such structures can be expressed in matrix form as[2]

$$\left[\mathbf{M}(x)\frac{\partial^2}{\partial t^2}+\mathbf{C}(x)\frac{\partial}{\partial t}+\mathbf{K}(x)\right]\left\{\begin{array}{c}\mathbf{w}(x,t)\\ \mathbf{v}(x,t)\end{array}\right\}=\left\{\begin{array}{c}\mathbf{f}_z(x,t)\\ \mathbf{f}_y(x,t)\end{array}\right\},\tag{1}$$

*Corresponding author. Tel.: +1-514-398-6280; fax: +1-514-398-7365.
E-mail address: mary.fiorilli@mcgill.ca (M.P. Païdoussis).
[1] Presently with the School of Technology, The College of the Bahamas, Nassau, Bahamas.
[2] In Refs. [1–3], for the sake of generality, these equations were presented in non-dimensional terms. Here they are presented dimensionally.

0022-460X/03/$ - see front matter
PII: S0022-460X(02)01219-1

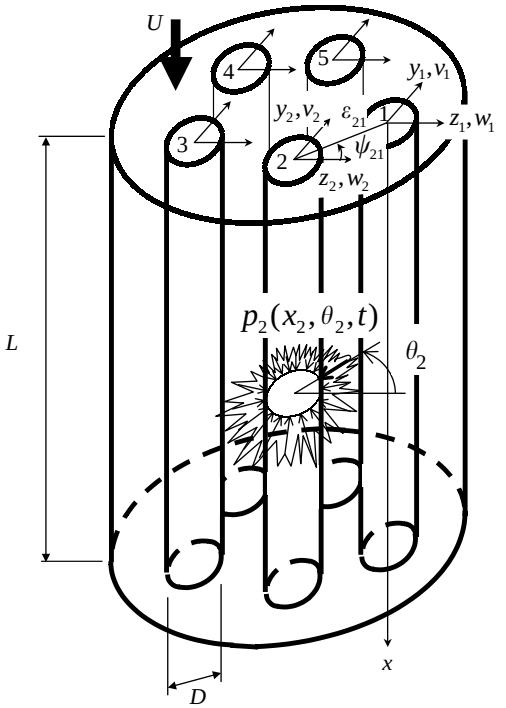

Fig. 1. Definition of Cartesian co-ordinates (x, y_r, z_r), lateral displacements (v_r, w_r) and azimuthal co-ordinate (θ_r) for cylinders in a channel; $r = 1, 2, \ldots, K$, where K is the number of cylinders in the channel. Pressure fluctuations are also illustrated laterally around cylinder 2. Ψ_{rs} is the angle subtended from the z_r axis by cylinder s; ε_{rs} is the distance between the centres of cylinders r and s.

where $\mathbf{M}(x)$, $\mathbf{C}(x)$ and $\mathbf{K}(x)$ are the mass, damping and stiffness matrices of the system, respectively, and they are square matrices; x, y, and z are the Cartesian co-ordinates illustrated in Fig. 1; t represents time; $\mathbf{w}(x, t)$ and $\mathbf{v}(x, t)$ are the vectors of lateral cylinder displacements from equilibrium in the z and y directions, respectively; $\mathbf{f}_z(x, t)$ and $\mathbf{f}_y(x, t)$ are the vectors of net lateral turbulent fluid forces per unit length acting on the walls of the cylinders in the z and y directions, respectively (see Appendix A).

2. The stochastic equations

2.1. The full equation

To obtain a solution for random cylinder vibration, manipulation of Eqs. (1) by a combination of Galerkin and Fourier methods gives rise to fluid force-per-unit-length cross-spectral densities (CSDs), which can be written in terms of a weighted double integral of the turbulent wall-pressure fluctuation CSDs around the circumferences of the cylinders [1,4,5]. Previously [3,6], measurements of the latter were obtained so that an analytical representation of the former can

now be achieved. This will be done shortly. The most general of the stochastic equations of which these forcing functions form a major part are as follows.

Writing for simplicity

$$\mathbf{f}(x,t) = \{\mathbf{f}_z(x,t), \mathbf{f}_y(x,t)\}^{\mathrm{T}}, \quad \boldsymbol{\eta}(x,t) = \{\mathbf{w}(x,t), \mathbf{v}(x,t)\}^{\mathrm{T}}, \tag{2}$$

the solution of Eq. (1) for random cylinder response can be written as [1,2]

$$R_{\eta_i\eta_j}(x,x',\bar{t}) = \frac{1}{2\pi}\int_{-\infty}^{\infty} S_{\eta_i\eta_j}(x,x',\Omega)\,\mathrm{e}^{\mathrm{i}\Omega\bar{t}}\,\mathrm{d}\Omega,$$

$$\begin{aligned} S_{\eta_i\eta_j}(x,x',\Omega) = \sum_{\ell=1}^{N}\sum_{n=1}^{N}\phi_\ell(x)\phi_n(x')\sum_{p=1}^{2KN}\sum_{q=1}^{2KN}\Big\{ & H^*_{\beta(\ell,i),p}(\Omega)H_{\beta(n,j),q}(\Omega) \\ & \times\int_0^L \mathrm{d}x_1\int_0^L \mathrm{d}x_2\,\phi_{a(p)}(x_1)\phi_{a(q)}(x_2)S_{f_{b(p)}f_{b(q)}}(x_1,x_2,\Omega)\Big\}, \\ & i,j = 1,2,\ldots,2K, \end{aligned} \tag{3}$$

where $R_{\eta_i\eta_j}(x,x',\bar{t})$ is the cross-correlation of $\eta_i(x,t)$ and $\eta_j(x',t)$, and $S_{\eta_i\eta_j}(x,x',\Omega)$ is defined as the corresponding CSD; $\phi_\ell(x)$, $\phi_n(x')$ are comparison functions which satisfy the boundary conditions of the problem;[3] N is the number of comparison function modes selected, K is the number of cylinders in the channel (see Fig. 1); $H_{\beta(\ell,i),p}(\Omega)$ and $H_{\beta(n,j),q}(\Omega)$ are elements of the frequency response function matrix of the system and are given by Eqs. (A.5b) and (A.3c)–(A.3e) in Appendix A with $W_{n'} = \phi_{n'}$ [1,4]; $S_{f_{b(p)}f_{b(q)}}(x_1,x_2,\Omega)$ is the CSD of $f_{b(p)}(x_1,t)$ and $f_{b(q)}(x_2,t)$; $\Omega = 2\pi f$, where f is frequency in Hz; $\bar{t}$ represents time delay in s; L is the cylinder length; $\beta(\ell,i) = 2K(\ell-1)+i$; $a(p) = \{\text{largest integer} \leqslant (2K+p-1)/2K\} = 1,2,\ldots$ or N, and $b(p) = p - 2K[a(p)-1] = 1,2,\ldots$ or $2K$. The derivation of Eq. (3) is given in Appendix A.

Now, certain practical applications may be such that the generality of Eq. (3) is unwarranted, and certainly in some situations (e.g., very large cylinder bundles and single-cylinder (annular) flows) the vast amount of numerical computation that ensues can be drastically reduced without excessive loss in accuracy and meaning of the results. Thus, special cases of Eq. (3), which are numerically more efficient, are to be utilized where advantageous. Some of these special cases now follow.

2.2. Case 1 (no excitation coupling)

Suppose, for instance, that inter-cylinder fluid excitation coupling is very much smaller than correlations between points on the same cylinder, which is the case in a relatively large and sparse cylinder bundle [3]. Then, the inter-cylinder cross terms of $S_{f_{b(p)}f_{b(q)}}(x_1,x_2,\Omega)$ in Eq. (3) are

[3] These are taken in the calculations as the Euler Bernoulli beam eigenfunctions.

negligible, and the equation reduces to

$$S_{\eta_i\eta_j}(x,x',\Omega)=\sum_{\ell=1}^{N}\sum_{n=1}^{N}\phi_\ell(x)\phi_n(x')\sum_{p=1}^{2KN}\sum_{n'=1}^{2N}\Bigg\{H^*_{\beta(\ell,i),p}(\Omega)H_{\beta(n,j),q'(n',p)}(\Omega)\times\int_0^L \mathrm{d}x_1\int_0^L \mathrm{d}x_2\,\phi_{a(p)}(x_1)\phi_{a(q'(n',p))}(x_2)S_{f_{b(p)}f_{b(q'(n',p))}}(x_1,x_2,\Omega)\Bigg\},\quad i,j=1,2,\ldots,2K, \tag{4}$$

where

$$q'(n',p)=\begin{cases}(n'-2)K+b(p), & b(p)>K,\\ (n'-1)K+b(p), & b(p)\leqslant K.\end{cases}$$

Eq. (4) is derived in detail in Appendix A. The number of summed elements indicated by n' (the 4th summation) has been reduced considerably compared to Eq. (3). Ignoring other parts of the overall calculation, this manipulation has resulted in computational savings of the order of $K:1$. For example, every hour of computation of the sums using Eq. (4) for a 16-cylinder bundle ($K=16$) corresponds to approximately 16 hours of computation for the same result using Eq. (3).

2.3. Case 2 (no excitation coupling—mode 1)

In addition to the above, assume that contributions by the first mode ϕ_1 to the cylinder response far outweigh those of higher modes $\phi_\ell;\ell>1$. Eq. (4) can then be further reduced to

$$S_{\eta_i\eta_j}(x,x',\Omega)=\phi_1(x)\phi_1(x')\sum_{p=1}^{2K}H^*_{ip}(\Omega)\sum_{n'=1}^{2}\Bigg\{H_{jq''(n',p)}(\Omega)\times\int_0^L \mathrm{d}x_1\int_0^L \mathrm{d}x_2\,\phi_1(x_1)\phi_1(x_2)S_{f_pf_{q''(n',p)}}(x_1,x_2,\Omega)\Bigg\},\quad i,j=1,2,\ldots,2K, \tag{5a}$$

where $H_{ip}(\Omega)$ are elements of the now unimodal frequency response function matrix

$$[H(\Omega)]=\left[\int_0^L\phi_1^2(x)[-\Omega^2\mathbf{M}(x)+\mathrm{i}\Omega\mathbf{C}(x)+\mathbf{K}(x)]\,\mathrm{d}x\right]^{-1} \tag{5b}$$

and

$$q''(n,p)=\begin{cases}(n'-2)K+p, & p>K,\\ (n'-1)K+p, & p\leqslant K.\end{cases}$$

This too is derived in Appendix A. Increased savings in computation of the sums over the full Eq. (3) has been achieved ($KN^4:1$), e.g., for every second of computation of the sums required by Eq. (5a) for a 16-cylinder bundle ($K=16$), approximately 6 h of computation would be required by Eq. (3) employing six modes ($N=6$), while Eq. (4) would require the order of 22 min.[4] Note that with $K=1$, Eq. (5a) reduces to the eccentric, annular flow problem.

[4] The reasoning that leads to this is as follows. Consider 1 s of computation using Eq. (5a). In Eq. (3) this corresponds to $KN^4=16\times6^4=20\,736$ s $=5.76$ h. Similarly, in Eq. (4) it corresponds to $5.76\text{ h}/K=5.76\text{ h}/16=0.36$ h $=21.6$ min.

2.4. Case 3 (no excitation and no response coupling)

In a third possibility, higher vibration modes remain important but all inter-cylinder fluid coupling (i.e., both excitation and response) becomes negligible [5]. Eq. (1) then becomes completely uncoupled and the matrices $\mathbf{M}, \mathbf{C}$ and $\mathbf{K}$ are diagonal. A multi-cylinder bundle can then be treated as one cylinder and one degree of freedom at a time [5]. Hence, from Eq. (3) we may write

$$S_{\eta_i\eta_i}(x,x',\Omega) = \sum_{\ell=1}^{N}\sum_{n=1}^{N}\phi_\ell(x)\phi_n(x')\sum_{p=1}^{N}\sum_{q=1}^{N}H_{\ell p}^{(i)*}(\Omega)H_{nq}^{(i)}(\Omega) \times \int_0^L \mathrm{d}x_1\int_0^L \mathrm{d}x_2\,\phi_p(x_1)\phi_q(x_2)S_{f_if_i}(x_1,x_2,\Omega), \quad i=1,2,\ldots,2K, \tag{6a}$$

where $H_{\ell p}^{(i)}(\Omega)$ are elements of the single-degree-of-freedom frequency response function matrix

$$[H^{(i)}(\Omega)] = \left[\int_0^L \begin{bmatrix} \phi_1(x)\phi_1(x) & \phi_1(x)\phi_2(x) & \cdots & \phi_1(x)\phi_N(x) \\ \vdots & \vdots & & \vdots \\ \phi_N(x)\phi_1(x) & \phi_N(x)\phi_2(x) & \cdots & \phi_N(x)\phi_N(x) \end{bmatrix} \times (-\Omega^2 M_{ii}(x) + \mathrm{i}\Omega C_{ii}(x) + K_{ii}(x))\,\mathrm{d}x\right]^{-1}. \tag{6b}$$

Eq. (6b) can be easily verified using Eq. (A.3) in Appendix A, and Equation (6a) can be derived using the method of Appendix A for a single-degree-of-freedom system. The savings in numerical computation of the sums realized here over the full Eq. (3) are of the order of $4K^2 : 1$.

2.5. Case 4 (no excitation and no response coupling—mode 1)

Finally, we consider non-eccentric annular flow. Here, the only two existing degrees of freedom are uncoupled, and assuming higher modes are also negligible, Eqs. (5a) and (6a) both reduce for first mode vibration to [7–9]

$$S_{\eta_1\eta_1}(x,x',\Omega) = \phi_1(x)\phi_1(x')H_{11}^{*}(\Omega)H_{11}(\Omega)\int_0^L \mathrm{d}x_1\int_0^L \mathrm{d}x_2\,\phi_1(x_1)\phi_1(x_2)S_{f_1f_1}(x_1,x_2,\Omega). \tag{7}$$

This is the simplest and most common of all these expressions. Consequently, the greatest savings obtain ($4K^2N^4 : 1$). All of the foregoing different possibilities are summarized together in Tables 1 and 2.

2.6. Temporal response and principal directions of vibration

The inverse Fourier transforms of the foregoing response spectral densities give rise to temporal response correlations, including r.m.s. vibration amplitudes (see Eq. (3)). There is a need, for the purpose of design, to study the relationships between dominant frequencies or frequency bands, in the system frequency response functions and the excitation spectral densities, to see how they interact, with respect to changing parameters such as flow velocity and cross-sectional geometry, to affect temporal observations such as r.m.s. vibration amplitudes and correlations [8,10]. This should be a consideration of future research.

Table 1
Summary of the full and reduced equations

Equation	Characteristics
(3)	Full, unabridged (FULL)
(4)	No inter-cylinder excitation correlation (NOINTEC)
(5a)	No inter-cylinder excitation correlation and first mode response only (NOINTEC 1)
(6a)	No inter-cylinder excitation correlation and no inter-cylinder response correlation (NOINTERC) (*This is identical to the problem of annular flow*)
(7)	Single cylinder annular flow and first mode response only (ANNULAR) (*This is the same as NOINTERC with* $N = 1$)

Table 2
Ratios of the number of terms in the summations—Eq. x : Eq. y

		Eq. y				
		(3)	(4)	(5a)	(6a)	(7)
Eq. x	(3)	1:1	K : 1 (16:1) (4:1)	KN^4 : 1 (20736:1) (324:1)	$4K^2$: 1 (1024:1) (64:1)	$4K^2N^4$: 1 (1327104:1) (5184:1)
	(4)		1:1	N^4 : 1 (1296:1) (81:1)	$4K$: 1 (64:1) (16:1)	$4KN^4$: 1 (82944:1) (1296:1)
	(5a)			1:1	$4K/N^4$: 1 (0.05:1) (0.2:1)	$4K$: 1 (64:1) (16:1)
	(6a)				1:1	N^4 : 1 (1296:1) (81:1)
	(7)					1:1

Upper parantheses values are for $K = 16, N = 6$; lower parantheses values are for $K = 4, N = 3$.

Also, since the cylinder vibrations are random, in both amplitudes and directions [8], further operations on $S_{\eta_i\eta_j}$ will be required to determine the preferred or principal planes or directions of oscillation where vibration amplitudes and correlations will be greatest and more focused [1,10–16].[5] The responses in any given directions around the cylinders can be determined, by resolving vectors, from those in the Cartesian directions [1,10].

[5] Recall that η_i and η_j are displacements in the fixed Cartesian directions illustrated in Fig. 1. The principal directions are not necessarily those defined as the Cartesian.

3. Characterization of differential wall-pressure CSDs

Differential wall-pressure CSDs constitute the force-per-unit length CSDs via the following equations [1,10]:

$$S_{f_i f_j}(x,x',f) = R^2 \int_0^{\pi}\int_0^{\pi} S_{\bar{p}_{r(i)}\bar{p}_{s(j)}}(x,x',\theta_r,\theta_s,f)\,Trig_i(\theta_r)\,Trig_j(\theta_s)\,\mathrm{d}\theta_r\,\mathrm{d}\theta_s,$$
$$i,j = 1,2,\ldots,2K, \tag{8}$$

where

$$r(i), s(j) = \begin{cases} i,j, & i,j \leqslant K, \\ i-K, j-K, & i,j > K \end{cases}$$

and R is the cylinder radius; $\bar{p}_{r(i)} = p_{r(i)}(x,\theta_r,t) - p_{r(i)}(x,\theta_r+180^\circ,t)$, the differential wall-pressure acting on the wall of the rth cylinder ($p_{r(i)}(\cdots)$ being the "point" wall-pressure and θ_r the azimuthal co-ordinate measured from Cartesian direction z_r—see Fig. 1); $S_{\bar{p}_{r(i)}\bar{p}_{s(j)}}(\ldots f)$ is the differential wall-pressure CSD between $\bar{p}_{r(i)}(x,\theta_r,t)$ and $\bar{p}_{s(j)}(x',\theta_s,t)$, $f = \Omega/2\pi$ (Hz);[6] and $Trig_i(\theta_r) = \cos\theta_r$ if $f_i(x,\theta_r,t)$ points in the z direction, $= \sin\theta_r$ if $f_i(x,\theta_r,t)$ points in the y direction (this depends on the value of i—see Eqs. (1) and (2)).

From previous measurements [3,6–8,16–22], it can be shown that it is possible to characterize to some degree the boundary layer differential wall-pressure CSD in a bundle of stationary cylinders by an expression of the following form:[7]

$$S_{\bar{p}_r\bar{p}_s}(x,x',\theta_r,\theta_s,f) \simeq S_{\overline{pp}}(x_0,\theta_0,f)/d_0\alpha_0\beta\left(\frac{fD_h}{U},\theta_r,\theta_s,\ldots\right)\gamma\left(\frac{fD_h}{U},\frac{|x-x'|}{D_h},\theta_s,\ldots\right)$$
$$\times\left\{d\left(\frac{fD_h}{U},\frac{x}{D_h},\theta_r,\ldots\right)d\left(\frac{fD_h}{U},\frac{x'}{D_h},\theta_s,\ldots\right)\alpha\left(\frac{fD_h}{U},\theta_r,\ldots\right)\right.$$
$$\left.\times\,\alpha\left(\frac{fD_h}{U},\theta_s,\ldots\right)\right\}^{1/2}\exp[-\mathrm{i}2\pi f(x'-x)/\bar{U}_c(\theta_s)], \quad r,s = 1,2,\ldots,K, \tag{9a}$$

where $S_{\overline{pp}}$ is a differential wall-pressure PSD on one of the cylinders in the bundle at a reference location (x_0,θ_0), and is given by[8]

$$S_{\overline{pp}}(x_0,\theta_0,f) \simeq \tfrac{1}{2} b_s \rho^2 U^3 D_h c^2 (D/D_h) d_0\alpha_0[P(\rho U D_h/\mu,\ldots)], \tag{9b}$$

where

$$d_0 = d(fD_h/U, x_0/D_h, \theta_0, \ldots), \quad \alpha_0 = \alpha(fD_h/U,\theta_0,\ldots) \tag{9c}$$

[6] Note that if point pressure CSDs, $S_{p_r p_s}$, are utilized in Eq. (8) instead of the differential ones, $S_{\bar{p}_r\bar{p}_s}$, the integrals should be taken from 0 to 2π instead of from 0 to π.

[7] See Eqs. (20) and (28a) of Ref. [3].

[8] Note that the physical measurements in Ref. [3] are of $G_{\overline{pp}}(\ldots f)$, the one-sided PSD, while $S_{\overline{pp}}(\ldots f)$, the two-sided PSD, is $\frac{1}{2}\times G_{\overline{pp}}(\ldots f)$, hence the factor of $\frac{1}{2}$ is here but not in Ref. [3]. Also, b_s from Ref. [3] has been replaced here by $b_s \times c^2(D/D_h)$, in order to reveal or rather separate the effect of confinement of the flow on the wall-pressure PSD, due to D/D_h [6].

where b_s is a system-dependent "quietness" function of proportionality (or bundle system "constant") which accounts for the differences in magnitude of the CSD (or PSD) from one system to another, ρ the fluid density, U the spatially averaged mean flow velocity, D_h the cross-sectional hydraulic diameter of the bundle, $D = 2R =$ cylinder diameter, c is a function that describes the effect of confinement on the wall-pressure CSDs [6]; P is a function that accounts for power level changes due to varying Reynolds number (Re), and the remaining functions β, γ, d, α and $\bar{U}_c$ are defined as follows [3]:

β a function, dependent mainly on $fD_h/U, \theta_r$ and θ_s, that accounts for the decay of correlation laterally between different points in the bundle ($\beta \to 1$ as $\theta_r \to \theta_s$ on the same cylinder and, in a laterally symmetric arrangement, $\beta = 0$ between points 90° apart on a given cylinder—see Appendix B, item 3)

γ a function, dependent mainly on fD_h/U, $|x - x'|$ and θ_s, that accounts for the decay of correlation longitudinally ($\gamma \to 1$ as $x' \to x$)

d a function (which is postulated to be dependent mainly on fD_h/U, x, x', θ_r and θ_s, as well as varying bundle entrance conditions [3,23,24]) that accounts for changes in the turbulent pressure field with distance travelled into the bundle before full development is reached (at full development, $d = 1$)

α describes the azimuthal variation in shape of the wall-pressure PSD around a cylinder and is dependent mainly on fD_h/U and θ

$\bar{U}_c(\theta_s)$ the average velocity of convection of wall-pressure disturbances longitudinally with the flow ($= (x' - x)/\bar{t}_c; x' \geqslant x$, where $\bar{t}_c$ is the time delay for correlation maximum between x and x'); it is only slightly influenced by azimuthal location of the longitudinal plane (i.e., θ_s)

Using the above definitions, a quick check shows that Eq. (9a) reduces to an identity when $x = x' = x_0$ and $\theta_r = \theta_s = \theta_0$, as it should.

Previously [3,6], it was found for a rectangular array of eight stationary cylinders, such as that illustrated in Fig. 2, that in the fully developed part of the flow, the following approximations hold:[9]

$$c \simeq [1 + (D/D_h)^{1.25}]^{-0.9}, \tag{10a}$$

$$P \simeq 1/Re = \mu/(\rho U D_h), \tag{10b}$$

$$\gamma \simeq \exp(-0.7f|\bar{x}|/U)[1 + \{\exp(-0.2f|\bar{x}|/U) - 1\}\sin^2 2\phi_s], \quad fD_h/U \geqslant 0.25, \tag{10c}$$

$$\alpha \simeq a'\{1 - \sin^2 2\phi_r[0.36 - 50(fD_h/U)^3 \exp(-3(fD_h/U)^2)]\}, \quad fD_h/U \geqslant 0.25 \tag{10d}$$

[9] In the absence of data to the contrary, the assumption will be that these functions remain more or less the same in the developing part of the flow, as in the fully developed part, for the sake of making sample calculations via Eq. (3). Furthermore, the expressions for γ, α and $\bar{U}_c$ are based only on data in the relatively low range of $Re = 6800$–$48\,000$ and at a fixed value of $D/D_h = 2.095$ [3].

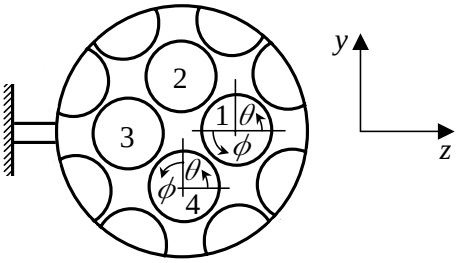

Fig. 2. Cross-section of the square array of eight cylinders in which the wall-pressure measurements of Eqs. (10a) to (10g) were made. The azimuthal co-ordinates ϕ in relation to θ [3,6] are defined.

and

$$\bar{U}_c(\theta_s) \simeq aU/[1 + f(\theta_s)], \quad fD_h/U \geqslant 0.25, \tag{10e}$$

where $\bar{x} = x' - x$; ϕ_r and ϕ_s are related to θ_r and θ_s as in Fig. 2; and

$$a' = \left[\left(1 - \left(\frac{fD_h}{3U}\right)^2\right)^2 + \left(2\zeta_1 \frac{fD_h}{3U}\right)^2\right]^{-1/2} + 31.986\left[\left(1 - \left(\frac{fD_h}{0.1349U}\right)^2\right)^2 + \left(2\zeta_2 \frac{fD_h}{0.1349U}\right)^2\right]^{-1/2},$$

$$\zeta_1 = 0.6, \quad \zeta_2 = 8.68582, \tag{10f}$$

$$a \simeq 1.129 \text{ (constant)} \quad \text{and} \quad f(\theta_s) \simeq 0.05 \sin^2 2\phi_s(\theta_s), \tag{10g}$$

$f(\theta_0)$ is notably a very weak function of θ_s. Also, as indicated, the above approximations are not valid for $fD_h/U < 0.25$ approximately. The error or uncertainty in the above equations was determined to be of the order of 20% [6]. Plots of γ versus $f\bar{x}/U$ (Eq. (10c)) have shown that the longitudinal correlation is significant over approximately 4 or 5 cycles ($f\bar{x}/\bar{U}_c \simeq f\bar{x}/1.129U \leqslant 4$ or 5) [3].

For the purpose of obtaining response calculations near zero frequency, the wall-pressure PSD and CSD in the small frequency range below $fD_h/U = 0.25$ are needed. In the absence of empirical data in this range, a reasonable estimate of the PSD will be obtained in this paper by linear extrapolation of that portion of the PSD measured above $fD_h/U = 0.25$ to zero magnitude at $fD_h/U = 0$. The justification for doing this will be given shortly. Lateral spectral density factors derived from the CSD will be treated similarly.

Finally, it was desirable to test the waters and apply the above approximations to other stationary cylinder bundles by utilizing Eqs. (10a), (10b), (10d) and (10f) as they are in Eq. (9b) in the fully developed region of the flow (i.e., where $d_0 = 1$) and determine the resulting values, or approximations, for b_s. This was done for a number of systems

from the literature and the results are summarized in Fig. 3(a), (b) and Table 3.[10] For calculation purposes the ranges of b_s shown may be arbitrarily extended on the low-frequency side to $fD_h/U = 0$, if it can be assumed that b_s inherently changes very little or even not at all with fD_h/U.

4. Empirical force-per-unit-length CSDs

Eq. (9a) may be substituted into Eq. (8) and the double integration performed to yield, for stationary cylinders,[11]

$$\frac{4S_{f_if_j}(x,x',f)}{\rho^2U^3D_hD^2} = \frac{S_{\overline{pp}}(x_0,\theta_0,f)}{\rho^2U^3D_hd_0\alpha_o}K_{ij}\left(\frac{fD_h}{U},\frac{x}{D_h},\frac{f|\bar{x}|}{U},\ldots\right)\exp(-\mathrm{i}2\pi f(x'-x)/(aU)),$$
$$i,j = 1,2,\ldots,2K, \tag{11}$$

where

$$K_{ij}\left(\frac{fD_h}{U},\frac{x}{D_h},\frac{f|\bar{x}|}{U},\ldots\right) = \int_0^\pi\int_0^\pi \beta(\ldots,\theta_r,\theta_s,\ldots)\gamma(\ldots,\theta_s,\ldots)$$
$$\times[d(\ldots,x,\theta_r,\ldots)d(\ldots,x',\theta_s,\ldots)\alpha(\ldots,\theta_r,\ldots)\alpha(\ldots,\theta_s,\ldots)]^{1/2}$$
$$\times\exp[-\mathrm{i}2\pi f(x'-x)f(\theta_s)/(aU)]\,Trig_i(\theta_r)Trig_j(\theta_s)\,\mathrm{d}\theta_r\,\mathrm{d}\theta_s,$$
$$r,s = r(i),s(j), \tag{12}$$

defined earlier in Eq. (8), and use has been made of Eq. (10e). Note that K_{ij} above is a complex function.

4.1. The differential pressure lateral spectral density factors (LASDF)

Neglecting the weak effect of θ_s on γ and $f(\theta_s)$, Eq. (12), reduces to

$$K_{ij} \simeq \gamma\left(\frac{fD_h}{U},\frac{\bar{x}}{D_h},\ldots\right)K_{ij,\theta}\left(\frac{fD_h}{U},\ldots\right), \tag{13}$$

where

$$K_{ij,\theta} = \int_0^\pi\int_0^\pi \beta(\theta_r,\theta_s)[\mathrm{d}(x,\theta_r)\,\mathrm{d}(x',\theta_s)\alpha(\theta_r)\alpha(\theta_s)]^{1/2}Trig_i(\theta_r)Trig_j(\theta_s)\,\mathrm{d}\theta_r\,\mathrm{d}\theta_s. \tag{14}$$

[10] It is, strictly speaking, not valid to use these correlation functions, particularly the wall-pressure PSD shape function given by $\alpha_o = a'$ (Eq. (10f)), in arbitrary cylinder bundles and tunnel systems, as geometric and other characteristic differences would render these functions slightly or perhaps greatly different from one system to another. In fact, the relatively large variance of b_s for the Clinch and Ohlmer et al. systems in Fig. 3(b) and Table 3, compared to the others, gives evidence that α_o, given by Eq. (10f), is less applicable to the Clinch and Ohlmer et al. systems than to the others. In order to alleviate, or rather characterize, the effects of some of these differences one might try to restrict the functions to a particular flow geometry and use turbulence correlation length scales to help characterize the turbulent pressure field over different bundle systems [6].

[11] This assumes that b_s of Eq. (9b) does not vary with location, θ, or is negligibly variant.

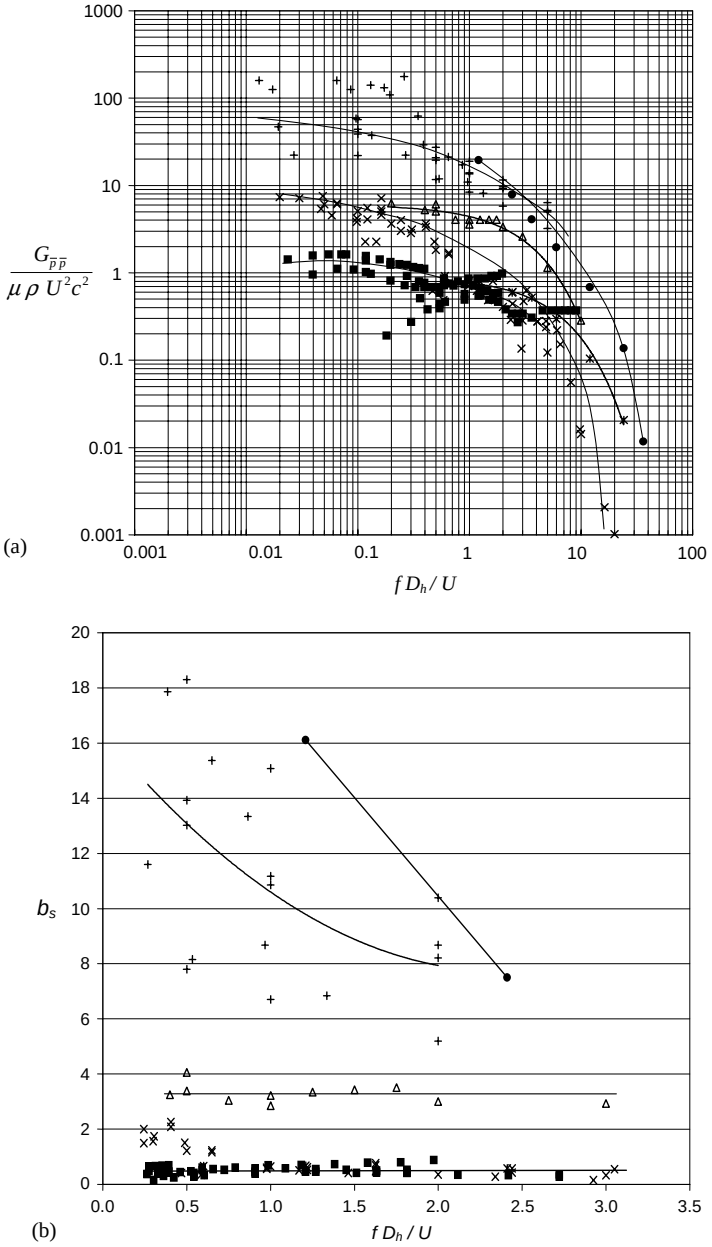

Fig. 3. Measured differential wall pressure PSD data from the literature: (a) normalized with respect to $\rho^2 U^3 D_h \times P(Re) \times [c(D/D_h)]^2$ to illustrate the scaling effect of b_s; (b) data of part (a) normalized by α_0 of Eq. (10f) to give estimates of b_s. In both (a) and (b): +, Ohlmer et al. [17,25]; ●, Clinch [20]; △, Curling and Païdoussis [3,6,26]; ×, Lin et al. [21] and Mulcahy et al. [22]; ∗, Bakewell et al. [18]; ■, Gagnon [unpublished].

γ is the longitudinal correlation decay function defined earlier, with the exception that the weak dependence on θ_s (see Eq. (10c)) has been neglected, so that γ could be factored out of the integrand of Eq. (12); γ is therefore considered to be responsible for variations of correlation in

Table 3
Estimates of b_s corresponding to wall-pressure data from the literature

Reference ($d_0 = 1, \alpha_0 = a'$ [of Eq. (10f)])	b_s	Range	Variation
Clinch [20]	12.0	$1.25 \leqslant fD_h/U \leqslant 2.5$	± 4.0
Ohlmer et al. [25,17]	12.0	$0.25 \leqslant fD_h/U \leqslant 2.0$	± 6.0
Curling and Paidoussis [3,6,26]	2.94	$0.25 \leqslant fD_h/U \leqslant 3.0$	$+1.0$ -0.2
Lin et al. [21], Mulcahy et al. [22]	0.6	$0.5 \leqslant fD_h/U \leqslant 3.0$	± 0.5
Bakewell et al. [18]	0.6	$0.5 \leqslant fD_h/U \leqslant 2.5$	± 0.1
Gagnon (unpublished)	0.5	$0.25 \leqslant fD_h/U \leqslant 3.0$	± 0.4

longitudinal planes only. $K_{ij,\theta}$ is a collective quantity and is termed the *differential pressure lateral spectral density factors* (*LASDF*) and is responsible for variations of correlation in lateral planes only.[12]

Note that $K_{ij,\theta}$ is a real function; note also that, by reason of d, it might reasonably be expected to vary in magnitude and shape with axial co-ordinates x and x', in the developing part of the flow [3,26]. In the fully developed region, however, where $d = 1$, it is invariant with changing axial location [3]. In what follows, the analysis will be restricted to the fully developed part of the flow.

If one sets $\bar{x} = x' - x = 0.0$ in Eq. (13) so that $\gamma = 1.0$ and K_{ij} reduces to $K_{ij,\theta}$, one obtains using Eqs. (11) and (9b) that

$$K_{ij,\theta} = \frac{4S_{f_i f_j}(x, x' = x, f) d_0 \alpha_0}{D^2 S_{\overline{pp}}(x_0, \theta_0, f)} = \frac{8S_{f_i f_j}(x, x' = x, f)}{\rho^2 U^3 D_h D^2 b_s c^2 P}. \tag{15}$$

Given the complexities of $\beta(\theta_r, \theta_s)$ for a bundle of cylinders [3] (as opposed to the much simpler cases of annular and pipe flows [7,8]) Eq. (15) is a welcome circumvention of the need for direct evaluation of Eq. (14), as $S_{f_i f_j}(x, x' = x, f)$ is a directly measurable quantity. In a previous analytical study, a so-called *shortest lateral fluid distance* (*SLFD*) point-pressure correlation scheme was utilized, enabling an analytical approximation for $K_{ij,\theta}$ (see the next section and also Refs. [1,10,16]). Here, however, an experimental determination of $K_{ij,\theta}$ will be made and contrasted with the previous SLFD scheme.

Shown in Fig. 4 are measurements of $8S_{f_i f_i}/(\rho^2 U^3 D_h D^2)$ at two different Reynolds numbers in the fully developed flow regime of a square array of eight stationary cylinders (see Fig. 2 and Ref. [3]). Approximating analytical curves have been fitted to the data. Due to cross-sectional geometric symmetry, the direction of f_i is arbitrary in this bundle with respect to the quantity measured (see Appendix B). Furthermore, by reason of Appendix B, on the same cylinder, the real function $K_{ij,\theta} = 0$ when $i \neq j$. Inter-cylinder excitation correlations are also negligible in this example [3]. Hence, in general, for all cylinders, $K_{ij,\theta} \simeq 0; i \neq j$, and the applicable analytical equation for the response is Eq. (4). The analytical approximation of the data in

[12] In pipe and annular flows, $\sqrt{K_{ij,\theta}}$ is related to Reavis' and Gorman's effective rod diameter [7,8]. It is a generalization of their "effective diameter ratio" for cylinder clusters.

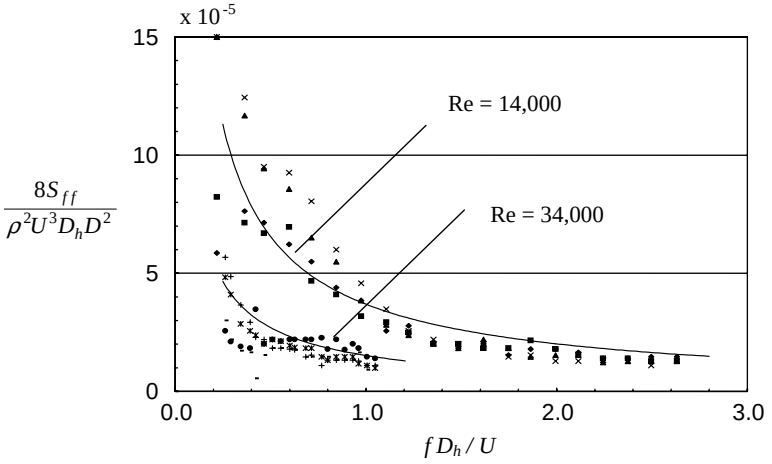

Fig. 4. Approximation of measured force-per-unit-length PSDs by Eq. (16). Data obtained in the bundle arrangement shown in Fig. 2 near mid-cylinder ($x/L = 0.494$) in the directions $\phi = 0^\circ$ and 90°, at two different Reynolds numbers, as shown. Different symbols are for the different ϕ and Re from two separate tests for repeatability; see Refs. [3,26].

Fig. 4 is given by

$$\frac{8S_{ff} \times Re}{\rho^2 U^3 D_h D^2} \simeq 7000 \exp\left[-10.13\left(\frac{fD_h}{U}\right)^{0.09}\right] + 17\,000 \exp\left[-11.18\left(\frac{fD_h}{U}\right)^{0.07}\right], \quad \frac{fD_h}{U} \geqslant 0.25. \tag{16}$$

This is applicable for $Re = 6800$–$48\,000$ and $D/D_h = 2.095$ [see footnote at Eq. (10a)]. Also, for this data we note [3,6] that $b_s = 2.94$ and $c = 0.322$ (using $D/D_h = 2.095$ in Eq. (10a)).[13] Thus, invoking Eqs. (15) and (10b), we obtain

$$\begin{aligned} K_{ij,\theta} &\simeq 22\,950 \exp\left[-10.13\left(\frac{fD_h}{U}\right)^{0.09}\right] + 55\,740 \exp\left[-11.18\left(\frac{fD_h}{U}\right)^{0.07}\right], \\ &\qquad i = j = 1, 2, \ldots, 2K; \;\; fD_h/U \geqslant 0.25 \\ &\simeq 0, \qquad i \neq j. \end{aligned} \tag{17a}$$

From Fig. 4, a margin of error of approximately 30% can be estimated. Note the applicable frequency range, $fD_h/U \geqslant 0.25$. The unspecified low frequency range from 0 to 0.25 will be treated as follows. First, Eq. (14) can, in principle, be evaluated at zero frequency, reasoning as follows. If there is no sensible lateral variation of static pressure throughout the bundle, diametrically opposing static pressures acting on the surface of a cylinder will be equal in magnitude and opposite in direction. The differential static component of wall-pressure will therefore equal zero. Consequently, in an infinitesimal frequency band at zero frequency the differential wall-pressure

[13] In Refs. [3,6], $b_s c^2 = 0.305$, hence the value given here for b_s. Also, depending on the explicit forms of the functions β, α, etc., or alternatively, the analytical expressions assumed for them, b_s may be found to vary somewhat with frequency and/or location in the bundle. In this case, it is relatively constant (see Fig. 3(b)).

PSD will be zero.[14] This leads to the conclusion that $\alpha_0 = 0$ in Eq. (9b) for all values of θ_0 at $fD_h/U = 0$, hence Eq. (14) evaluates to zero at $fD_h/U = 0$. For calculation purposes, a linear variation (''descent to zero'') of LASDF is then assumed between $fD_h/U = 0$ and 0.25, and since the gap, 0 to 0.25, is relatively small, this assumption should involve minimal error. Accordingly,

$$K_{ij,\theta} \simeq \frac{K_{ij,\theta}(fD_h/U = 0.25)}{0.25} \times \frac{fD_h}{U} = 20.75\frac{fD_h}{U}, \quad i = j \text{ and } 0 \leqslant fD_h/U < 0.25. \tag{17b}$$

The differential pressure LASDF, $K_{ij,\theta}$, as quantified by Eqs. (17a) and (17b) is illustrated in Fig. 5(a) where comparisons are also made to a previous approximation for the point pressure LASDF, $K''_{ij,\theta}$, obtained using pipe and annular flow pressure measurements (see the SLFD correlation scheme later) and a ''PSD-factored'' differential pressure LASDF, $K'_{ij,\theta}$ (see Eq. (20b) later).

4.2. The longitudinal spectral density factors (LOSDF) and final formulation of the response

Eqs. (11) and (13) are combined to yield

$$\frac{4S_{f_if_j}(x_1, x_2, f)}{\rho^2 U^3 D_h D^2} = \frac{S_{\overline{pp}}(x_0, \theta_0, f)}{\rho^2 U^3 D_h d_0 \alpha_0} K_{ij,\theta}\left(\frac{fD_h}{U}, \ldots\right)\gamma\left(\frac{fD_h}{U}, \frac{\bar{x}}{D_h}, \ldots\right) \times \exp[-\mathrm{i}2\pi f(x_2 - x_1)/(aU)], \quad i,j = 1, 2, \ldots, 2K, \tag{18}$$

where x_1 and x_2 are dummy variables replacing x and x', and $\bar{x} = x_2 - x_1$. Recall that this equation represents the fluid excitation forces acting on rigid, stationary cylinders. One now invokes the quasi-static assumption where, if the vibration is sufficiently small, the excitation on moving cylinders is approximately the same as that on corresponding stationary ones. Substituting Eq. (18) into Eq. (3) written in terms of $f = \Omega/2\pi$, one obtains

$$\frac{4d_0\alpha_0 S_{\eta_i\eta_j}(x, x', f)}{D^2 S_{\overline{pp}}(x_0, \theta_0, f)} = \sum_{\ell=1}^{N}\sum_{n=1}^{N} \phi_\ell(x)\phi_n(x') \sum_{p=1}^{2KN}\sum_{q=1}^{2KN} H^*_{\beta(\ell,i),p}(f) H_{\beta(n,j),q}(f) \times K_{b(p)b(q),\theta}\left(\frac{fD_h}{U}, \ldots\right) K_{a(p)a(q),x}\left(\frac{fD_h}{U}, \ldots\right), \quad i,j = 1, 2, \ldots, 2K, \tag{19a}$$

[14] Alternatively, it can be stated that we are concerned only with dynamic differential pressures. Therefore, the static component can be neglected. Nevertheless, it is to be emphasized that the ''zero-frequency/zero-PSD'' assumption depends on the static pressure balancing out in the differential pressure measurements, as stated from the outset. Moreover, under this condition, the same conclusion can be reached in a different way, as follows. In terms of point pressure PSDs and CSDs, the differential pressure PSD can be written as [26] $G_{\overline{pp}} = G_{(p_1-p_2)(p_1-p_2)} = (G_{p_1p_1} + G_{p_2p_2}) - (G_{p_1p_2} + G_{p_2p_1})$, where p_1 and p_2 are diametrically opposed point pressures. Two facts should be noted. First, there is no convection of disturbances laterally. Hence, in a lateral plane the CSD is real (i.e., not complex) and $G_{p_1p_2} = |G_{p_1p_2}| = G_{p_2p_1} = |G_{p_2p_1}|$. Second, at zero frequency, or more precisely, in an infinitesimal frequency band at zero frequency, the point static pressure is, by definition, fully coherent around and along the cylinder (this is corroborated by the fact that point pressure measurements of β and γ all tend to 1.0 as frequency tends to zero—see Eqs. (21b) and (21c) later). Together these two facts imply that $G_{p_1p_2} = G_{p_2p_1} = \sqrt{G_{p_1p_1}}\sqrt{G_{p_2p_2}}$ in the above at zero frequency, and leads to the factorization, $G_{\overline{pp}} = (\sqrt{G_{p_1p_1}} - \sqrt{G_{p_2p_2}})^2$. When the static pressure balances diametrically, $G_{p_1p_1} = G_{p_2p_2}$, and hence $G_{\overline{pp}} = 0$ at zero frequency.

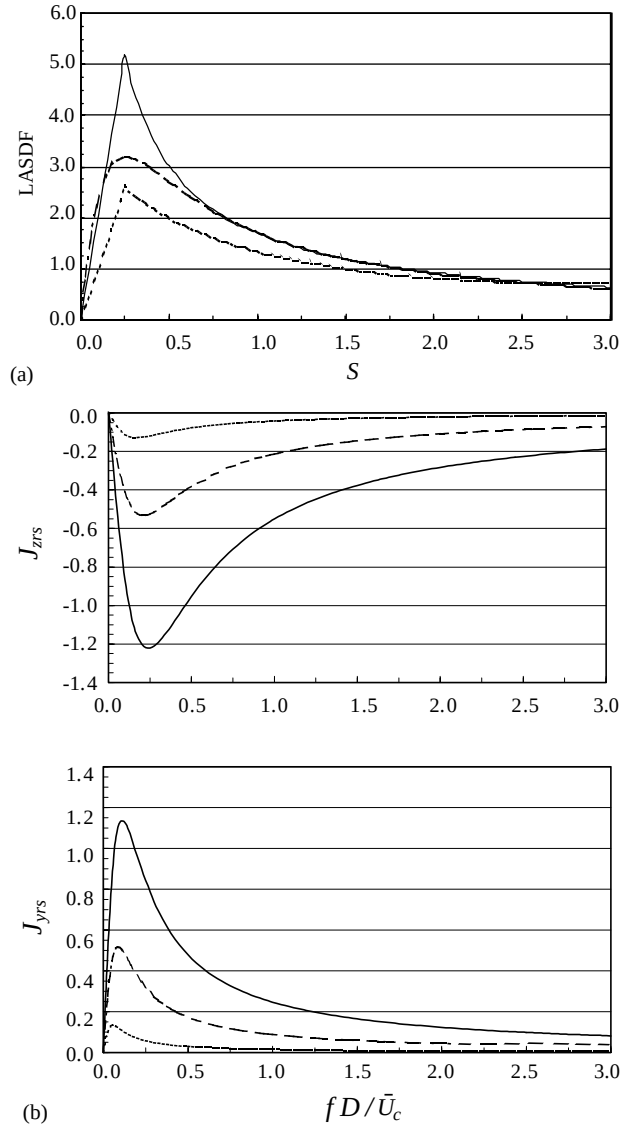

Fig. 5. (a) LASDF versus reduced frequency for the same cylinder ($r = s$), with $i = j$, by the empirical and SLFD correlation schemes: ——, empirical scheme, $K_{ij,\theta}$, Eqs. (17a) and (17b), and $S = fD_h/U$; ⋯, empirical scheme, $K'_{ij,\theta}$, Eq. (20b) and $S = fD_h/U$; – – –, SLFD scheme, $K''_{ij,\theta}$, Eq. (23a) and $S = fD/\bar{U}_c$. (b) LASDF versus reduced frequency for different cylinders ($r \neq s$) by the SLFD scheme [$K''_{ij,\theta}$, represented by J_{zrs} and J_{yrs}, Eq. (23a)]: ——, $\varepsilon_{rs} = 2$; – – –, $\varepsilon_{rs} = 3$; ⋯, $\varepsilon_{rs} = 6$.

where

$$K_{a(p)a(q),x}\left(\frac{fD_h}{U}, \ldots\right) = \int_0^L \mathrm{d}x_1 \int_0^L \mathrm{d}x_2\, \phi_{a(p)}(x_1)\phi_{a(q)}(x_2)\gamma\left(\frac{fD_h}{U}, \frac{x_2 - x_1}{U}, \ldots\right) \times \exp[-\mathrm{i}2\pi f(x_2 - x_1)/(aU)], \quad a(p), a(q) = 1, 2, \ldots, N. \tag{19b}$$

These quantities ($K_{a(p)a(q),x}$) are defined collectively as the longitudinal spectral density factors (LOSDF) [1,10], elsewhere also called "acceptance" [27]. In keeping with the nomenclature of Reavis [7] and Gorman [8], when $a(p) = a(q) = 1$, the real part of Eq. (19b) reduces to $L^2\Psi_L^2$, where Ψ_L refers to the ratio of an effective rod length to actual rod length (obtained by factoring out L^2 from the integration—see Appendix C). Eq. (19b) is a generalization of the "effective rod length" for cylinder clusters. Details of the evaluation of $K_{a(p)a(q),x}$, when γ is an exponential function as it is here when the minute effects of θ are neglected (i.e., set $\phi_s = 0$ in Eq. (10c)), and the $\phi_{a(p)}$'s are the Euler–Bernoulli beam eigenfunctions, can be found in Refs. [10,14] and to some extent in Refs. [7,28]. See Appendix C for a summary. Since low-frequency effects ($fD_h/U < 0.25$) have already been accounted for by $K_{ij,\theta}$, the range of γ (i.e., Eq. (10c)) and hence $K_{\ell n,x}$ will be extended in the calculations to $fD_h/U = 0$, noting that γ should in any case tend to 1.0 as f tends to zero. A similar rationale applies to $\bar{U}_c(\theta_s)$ (Eq. (10e)).

4.3. An alternative formulation of the response

By repositioning $d_0\alpha_0$, Eq. (19a) can obviously be alternatively written as

$$\frac{4S_{\eta_i\eta_j}(x,x',f)}{D^2S_{\overline{pp}}(x_0,\theta_0,f)} = \sum_{\ell=1}^{N}\sum_{n=1}^{N}\phi_\ell(x)\phi_n(x')\sum_{p=1}^{2KN}\sum_{q=1}^{2KN}H^*_{\beta(\ell,i),p}(f)H_{\beta(n,j),q}(f)K'_{b(p)b(q),\theta}\left(\frac{fD_h}{U},\ldots\right) \times K_{a(p)a(q),x}\left(\frac{fD_h}{U},\ldots\right), \quad i,j = 1,2,\ldots,K, \tag{20a}$$

where

$$K'_{b(p)b(q),\theta}\left(\frac{fD_h}{U},\ldots\right) = \frac{K_{b(p)b(q),\theta}(fD_h/U,\ldots)}{d_0\alpha_0}, \tag{20b}$$

a "normalized" LASDF, and $K_{a(p)a(q),x}(fD_h/U,\ldots)$ is the same as before. Both expressions (19a) and (20a) have merit. In the first, the "normalized" wall-pressure PSD, $S_{\overline{pp}}(x_0,\theta_0,f)/d_0\alpha_0$, is independent of $d_0\alpha_0$ and therefore is transferable between systems with different $d_0\alpha_0$ characteristics, while $K_{ij,\theta}$ is dependent on $d_0\alpha_0$ and is therefore not transferable. In the second, $S_{\overline{pp}}(x_0,\theta_0,f)$ is dependent on $d_0\alpha_0$ and is not transferable, while the "normalized" LASDF, $K'_{ij,\theta}$, does not depend on $d_0\alpha_0$ and therefore is a bit more transferable than the "unnormalized" LASDF.[15] This will be borne out in the sample calculations presented later. $K'_{ij,\theta}$ is shown graphically in Fig. 5(a), for $d_0 = 1$ and α_0 given by Eq. (10d) with $\phi_r = 0$ [i.e., α_0 is given by Eq. (10f)].[16]

[15] In other words, for two different bundles, the assumption is that the normalized quantities, $K'_{ij,\theta}$ and $S_{\overline{pp}}(x_0,\theta_0,f)/d_0\alpha_0$, are the same in both, whereas the unnormalized quantities, $K_{ij,\theta}$ and $S_{\overline{pp}}(x_0,\theta_0,f)$, may be different in both. Unfortunately, the two normalized quantities cannot be used simultaneously, therefore the choice has to be made between normalizing the PSD and normalizing the LASDF. The sample calculations explore both choices.

[16] As in Eqs. (17a) and (17b), $K'_{ij,\theta} = 0$ when $i \neq j$, for the eight-cylinder system under consideration.

5. The SLFD wall-pressure and force-per-unit length CSDs

5.1. Point pressure correlations and CSDs

The shortest lateral fluid distance (SLFD) force-per-unit-length CSDs of a previous study [1,14] stem from single-cylinder and pipe-flow, point[17] wall-pressure correlation measurements [18–20,22,29] and, an assumed inter-cylinder point wall-pressure correlation scheme [1,10,16]. In a single-cylinder system, measurements have shown that point wall-pressure correlations between two different points in a lateral plane on the cylinder decay in strength with the shortest distance between the two points around the circumference of the cylinder. Measurements of lateral point wall-pressure correlations being unavailable for bundles of cylinders at the time of developing this model of the correlations, the assumption was made that, in a bundle, the point wall-pressure correlations on stationary cylinders between any two points in a lateral plane decay in strength with the shortest lateral distance through the fluid between the two points. Thus, the lateral decay function for points on the same (stationary) cylinder is taken in the model to be that of the single-cylinder (annular flow) measurements, which are similar to and hence approximated by those measured in pipe flow [7,8,10,17–20,22,28–31]. The lateral decay function for points on different (stationary) cylinders in the bundle is taken to be of the same form as that measured around the circumference of a single cylinder or inner pipe wall, but having the distances around the cylinder walls and shortest extension out into the fluid from a point on one cylinder to a point on the next as the spatial separation parameter. This is done without regard for the presence of obstructions, such as other cylinders, along the shortest path through the fluid, for the sake of simplicity. This simplification has negligible impact on the cylinder vibration calculations if inter-cylinder correlations beyond the nearest neighbouring cylinders are negligible, which is indeed the case in the set of empirical correlations given in the previous section of this paper, in which all inter-cylinder wall-pressure correlations are negligible.

Wall-pressure correlations in the longitudinal direction on cylinders in a bundle are taken to be the same as those measured in the longitudinal direction on a single cylinder (annular flow) and in pipe flow. Thus, the pressure field in annular and pipe-flow systems being characteristically homogeneous, the bundle-flow longitudinal correlations are assumed to be the same in all longitudinal planes on all cylinders in the bundle, which is a reasonable approximation in the light of the preceding empirical longitudinal correlations, where the effects of ϕ_s (azimuthal co-ordinate) on the longitudinal correlation functions, γ and $\bar{U}_c$ are small [see Eqs. (10c) and (10e)]. Correlation decay in oblique directions, whether between points on the same cylinder in the bundle or between points on different cylinders, is represented by the product of the lateral and longitudinal decay functions. (This independent-planes model of the pressure field for oblique directions was first suggested by Corcos [32] based on existing measurements and is justified analytically here in Appendix D.) Putting all of this together, the SLFD wall-pressure CSD for point pressures in the cylinder bundle in the fully developed flow region can be written as [1,10,16]

$$S_{p_r p_s}(x, x', \theta_r, \theta_s, f) \simeq S_{pp}(f)\beta(S_\theta)\gamma(S_x)\mathrm{e}^{-\mathrm{i}2\pi S_x}, \tag{21a}$$

[17] "Point" as opposed to "differential", as discussed in the preceding.

where, using the Bakewell [18] and Bakewell [19] pipe-flow correlation functions,

$$\beta(S_\theta) = (1 + cS_\theta^2)^{-1}[2 - \exp(-dS_\theta^2)]^{-1}, \tag{21b}$$

$$\gamma(S_x) = \exp(-b|S_x|), \tag{21c}$$

$$S_x = \frac{f(x' - x)}{\bar{U}_c}, \quad S_\theta = \frac{fL_{min}(\theta_r, \theta_s)}{\bar{U}_c}, \tag{21d}$$

$$100\,000 \leqslant Re \leqslant 300\,000; \;\; D/D_h \to 0.$$

$L_{min}(\theta_r, \theta_s)$ is the shortest lateral fluid distance between the points (x, θ_r) and (x', θ_s). $\bar{U}_c$, the average, frequency-dependent pressure disturbance convection velocity between x and x', is independent of lateral co-ordinates (a characteristic of pipe and annular flows—taken here as being equal to the bulk channel flow velocity U for the frequency range of interest [14,16]—cf. Eq. (10e)), the constants $(b, c, d) = (0.7, 10, 80)$ and $S_{pp}(f)$ is the point reference or "signature" wall-pressure PSD of the system similar to its differential counterpart discussed earlier. Note that $S_{pp}(f)$ corresponds to $\frac{1}{2}S_{\overline{pp}}(x_0, \theta_0, f)$ (Eq. (9a)) discussed earlier[18] and is invariant with θ_0, as the correlation functions in this scheme were derived from pipe and annular flow correlations where the pressure field is characteristically homogeneous with respect to lateral co-ordinate, θ. Note that $\beta(S_\theta)$ tends to unity as the reduced frequency S_θ tends to zero, as expected [see footnote preceding Eq. (17b)]. This model of the pressure field is "exact" for a single-cylinder annular-flow system, wherein inter-cylinder correlations become irrelevant. It is used here in bundles of cylinders for comparison purposes and as a guide to the development of a more elaborate empirical model for bundles. Accordingly, Eq. (21a) is to be compared to Eq. (9a). In Eq. (9a), the generalizations from fully developed, homogeneous, pipe and annular flows, required by bundle flows (i.e., clusters of cylinders), are evident. The form of Eq. (9a) reduces to that of Eq. (21a) for a fully developed flow around a single-cylinder system, as it should.

5.2. Point pressure LASDF and LOSDF, and the SLFD formulation of the response

The operations required by Eq. (8) for point pressures integrated completely around the cylinders (θ_r, θ_s from 0 to 2π) can be carried out using the above SLFD point pressure correlation scheme (Eqs. (21a)–(21d)) and the result utilized in Eq. (3), under the quasi-static assumption, to yield an equation similar to Eqs. (19a) and (20a), i.e.,

$$\frac{4S_{\eta_i\eta_j}(x, x', f)}{D^2 S_{pp}(f)} = \sum_{\ell=1}^{N}\sum_{n=1}^{N} \phi_\ell(x)\phi_n(x') \sum_{p=1}^{2KN}\sum_{q=1}^{2KN} H^*_{\ldots} H_{\ldots} K''_{\ldots,\theta} K''_{\ldots,x}, \tag{22a}$$

where, the missing subscripts being the same as in Eq. (19a),

$$K''_{ij,\theta} = \int_0^{2\pi}\int_0^{2\pi} \beta(S_\theta) Trig_i(\theta_r) Trig_j(\theta_s)\, \mathrm{d}\theta_r\, \mathrm{d}\theta_s, \quad i,j = 1, 2, \ldots 2K \tag{22b}$$

[18] Assuming that it is valid to take differential PSDs as being twice the corresponding point PSDs [3,14].

(this is the point pressure LASDF—cf. Eq. (14)) and

$$K''_{\ell n,x} = \int_0^L \int_0^L \phi_\ell(x)\phi_n(x')\gamma(S_x)\,\mathrm{e}^{-\mathrm{i}2\pi S_x}\,\mathrm{d}x\,\mathrm{d}x', \quad \ell, n = 1, 2, \ldots, N \tag{22c}$$

(this is the point pressure LOSDF—cf. Eq. (19b)). Numerically evaluating Eq. (22b), coupled with Eq. (21b), and curve fitting the result yields the following analytical approximation for the point pressure LASDF [10,14,16]:

$$\begin{aligned} K''_{ij,\theta} &\simeq \frac{a_1|S_R|}{(1+a_2S_R^2)}(1+\mathrm{e}^{-a_3|S_R|}) \quad \text{if } r(i)=s(j) \text{ and } i=j \\ &= 0 \quad \text{if } r(i)=s(j) \text{ and } i\neq j \\ &\simeq Trig_i(\Psi_{rs})Trig_j(\Psi_{rs})J_{zrs} + [N_{ij} - Trig_i(\Psi_{rs})Trig_j(\Psi_{rs})]J_{yrs} \quad \text{if } r(i)\neq s(j), \end{aligned} \tag{23a}$$

where $r, s = r(i), s(j)$ and $Trig_i$ are defined in Eq. (8), $S_R = fR/\bar{U}_c$; the angle Ψ_{rs} is defined in Fig. 1, and where

$$N_{ij} = \begin{cases} 1 & (\text{both } i \text{ and } j \leqslant K) \text{ or } (\text{both } i \text{ and } j > K), \\ 0 & \text{otherwise}, \end{cases} \tag{23b}$$

$$(a_1, a_2, a_3) = (38.344, 40.611, 19.091), \tag{23c}$$

$$J_{zrs} = \frac{b_1\varepsilon_{rs}^{c_1}|S_R|}{(1+b_2\varepsilon_{rs}^{c_2}S_R^2)}(1+\mathrm{e}^{-b_3|S_R|}) \tag{23d}$$

with

$$(b_1, b_2, b_3) = (-33.795, 44.342, 0.06283), \quad (c_1, c_2) = (-1.7348, 0.62895). \tag{23e}$$

J_{yrs} is similar to J_{zrs} but with the constants

$$(b_1, b_2, b_3) = (52.183, 140.666, 0.03942), \quad (c_1, c_2) = (-1.3449, 1.2100), \tag{23f}$$

$$\varepsilon_{rs} = R_{rs}/R, \tag{23g}$$

where R_{rs} is the distance between centres of cylinders r and s, and $R = D/2$, cylinder radius.

$K''_{ij,\theta}$ as given above is valid for $-50 \leqslant S_R \leqslant 50$ and $2 \leqslant \varepsilon_{rs} \leqslant 6$. Components of the point pressure $K''_{ij,\theta}$ by the SLFD scheme are illustrated in Figs. 5(a) and (b), where a comparison is also made in Fig. 5(a) to the empirical differential schemes discussed earlier.

The LOSDF, $K''_{\ell n,x}$, are of the same form as given previously (Eq. (19b) with $a = 1, U = \bar{U}_c$). Examples of the evaluated integrals for LOSDF can be found in Refs. [10,14] and to some extent in Refs. [7,28]. See Appendix C for a summary.

The similarities among the response equations (19a), (20a) and (22a) are to be particularly noted. The only significant differences lie in the use of point or differential wall-pressure schemes and the interpretations and characterizations of the wall-pressure PSD and the lateral and longitudinal spectral density factors.

6. The single-cylinder stochastic response equation

Considering annular flows ($i,j = 1,2$), simplifying to the first mode and assuming no fluid coupling between the two degrees of freedom (i.e., zero eccentricity), Eq. (19a) reduces significantly to

$$S_{\eta_1\eta_1}(x,x',f) = \frac{D^2 S_{\overline{pp}}(x_0,\theta_0,f)}{4d_0\alpha_0}\,\phi_1(x)\phi_1(x')H_{11}^*(f)H_{11}(f)K_{11,\theta}(f)K_{11,x}(f). \tag{24}$$

This also follows from Eqs. (7), (18) and (19b). An equation like this has been derived by Thomson [9].

This equation can also be written in terms of $K'_{11,\theta}$ (see Eqs. (20a) and (b)), as well as $S_{pp}(x_0,\theta_0,f)$, $K''_{11,\theta}$ and $K''_{11,x}$ (see Eqs. (22a)–(22c)). The latter form, using different terminology from the above, has been derived and utilized previously by Reavis [7] and Gorman [8].

7. Sample calculations of the cylinder response spectra

Sample calculations are presented for the response of the four-cylinder system ($K = 4$) described in Ref. [16] and shown here in cross-section in Fig. 6. Measurements of the response of this system are available for comparison with theory. The system has clamped–clamped boundary conditions, $\rho = 1000$ kg/m^3, $\mu = 0.00101$ Ns/m^2, $D = 25.3$ mm, $D_h = 128.6$ mm, $m = 0.577$ kg/m, $L = 470$ mm, $E = 2780$ kPa, and $G_c = 0.75$; these parameters are, respectively, the fluid density, viscosity, cylinder diameter, hydraulic diameter, cylinder mass per unit length, cylinder length, modulus of elasticity and smallest inter-cylinder gap divided by cylinder radius. From unpublished data by Gagnon, b_s for this system is approximately 0.5 ± 0.4 (see Fig. 3(b) and Table 3). The response will be determined at flow velocity $U = 2.13$ m/s, or non-dimensionally, $u = 3.0$ [16].[19]

7.1. The response using Eq. (19a)

The differential wall-pressure PSD is given by Eq. (9b) which, using Eqs. (10a) and (10b), reduces to

$$S_{\overline{pp}}(x_0,\theta_0,f) \simeq \tfrac{1}{2} b_s \rho\mu U^2 d_0\alpha_0[1 + (D/D_h)^{1.25}]^{-1.8}. \tag{25}$$

Inserting the values for the $K = 4$ system described above, this becomes

$$\frac{S_{\overline{pp}}(x_0,\theta_0,f)}{d_0\alpha_0} \simeq 9.153 \times 10^{-7}\ \text{kPa}^2/\text{Hz}. \tag{26}$$

Using this in Eq. (19a), the response PSDs and CSDs, $S_{\eta_i\eta_j}(\ldots)/D^2$, of mid-cylinder displacements were calculated on the computer.[20] The results, plotted versus reduced (or scaled) frequency ω, are shown in Figs. 7 and 8. ω (measured in rad) is related to frequency $f = \Omega/2\pi$ (Hz) by the equation

$$\omega = 2\pi L^2[(m + \rho A)/EI]^{1/2} f = 6.1016f, \tag{27a}$$

[19] *Re* for this example is approximately 270 000—well beyond the range of the empirical expressions of Sections 3 and 4 but not outside that of the expressions of Section 5. Additionally $D/D_h = 0.197$, compared to 2.095 for some of the expressions of Sections 3 and 4, and 0.0 for the pipe-flow based expressions of Section 5.

[20] As stated earlier, these calculations neglect the developing part of the flow, characterized by $d(fD_h/U, \ldots)$.

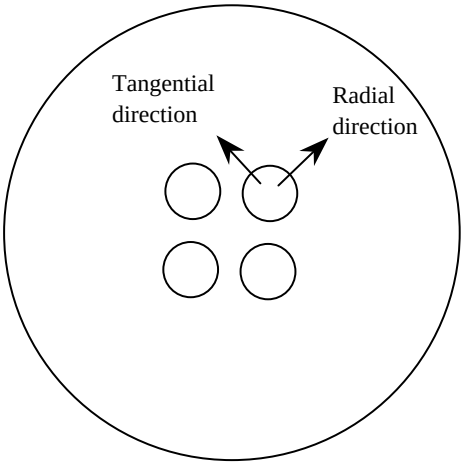

Fig. 6. Cross-section of the four-cylinder system used in experiments [16] for which the sample calculations of Section 7 were made. Radial and tangential directions are defined.

where I is the area moment of inertia of the cylinder ($= \pi D^4/64$). The CSDs are shown in the form of coherences, i.e., $|\mathrm{CSD}_{1,2}|^2/(\mathrm{PSD}_1 \times \mathrm{PSD}_2)$, and phases. Conforming with the definitions used in Ref. [16], the PSDs are shown as

$$G'_{\eta_1\eta_1} = \frac{\Omega}{2\pi\omega} G_{\eta_1\eta_1} = \frac{\Omega}{\pi\omega} S_{\eta_1\eta_1}, \tag{27b}$$

where $S_{\eta_1\eta_1}$ is defined by Eq. (3).[21]

Experimental measurements of the response by Gagnon and Païdoussis [16] are also shown in Figs. 7 and 8 for comparison with the theoretical response. While experimental and theoretical coherences tend to agree very well (Fig. 8—(see also Refs. [1,2,16]), the theoretical PSDs (Fig. 7) clearly overestimate the experimental ones at the important first mode frequencies, by factors exceeding 20, too great for practical use. This large discrepancy could possibly be attributed to a number of reasons, including but not limited to the following: (1) the specific dependence of $K_{ij,\theta}$ on the system (mainly its cross-sectional geometric configuration) in which it was measured, (2) the wide margin of error associated with $b_s(\pm 80\%)$, and (3) the differences in Re and D/D_h between the excitation used in the theory ($Re = 6800$–$48\,000$; $D/D_h = 2.095$) and the experimental four-cylinder system ($Re = 270000$; $D/D_h = 0.197$).[22] The foregoing calculations attempted to transfer $K_{ij,\theta}$ from a densely populated eight-cylinder bundle (Fig. 2) to the more sparsely populated four-cylinder one (Fig. 6). The inapplicability of $K_{ij,\theta}$ to the four-cylinder bundle and large error in b_s have contributed to the large differences in the theoretical and experimental

[21] In contrast to Eq. (3), the definition used in the non-dimensional version of the theory is $R_{\eta_i\eta_j}/D^2 = (1/2\pi)\int_{-\infty}^{\infty}(S''_{\eta_i\eta_j}/D^2)\exp(\mathrm{i}\omega\bar{\tau})\,\mathrm{d}\omega$ [1,10]. The link between this and Eq. (3) is the constant ratio, Ω/ω, giving $S'' = (\Omega/\omega)S$. In Ref. [16], an additional factor of 2π was employed for the one-sided spectrum, $G' = 2S'$, giving $G' = (1/2\pi)G'' = (1/\pi)S'' = (\Omega/\pi\omega)S$.

[22] A quick sketch of $c^2(D/D_h)$ vs D/D_h illustrates how significantly D/D_h affects the wall-pressure PSD at large D/D_h. Since the empirical expressions of Section 3 were obtained only at a single value of $D/D_h(= 2.095)$ we still do not know whether changing D/D_h also significantly affects the remaining parts of the excitation. Specifically, γ, $\bar{U}_c \to K_{ln,x}$ and $\alpha, \beta \to K_{ij,\theta}$.

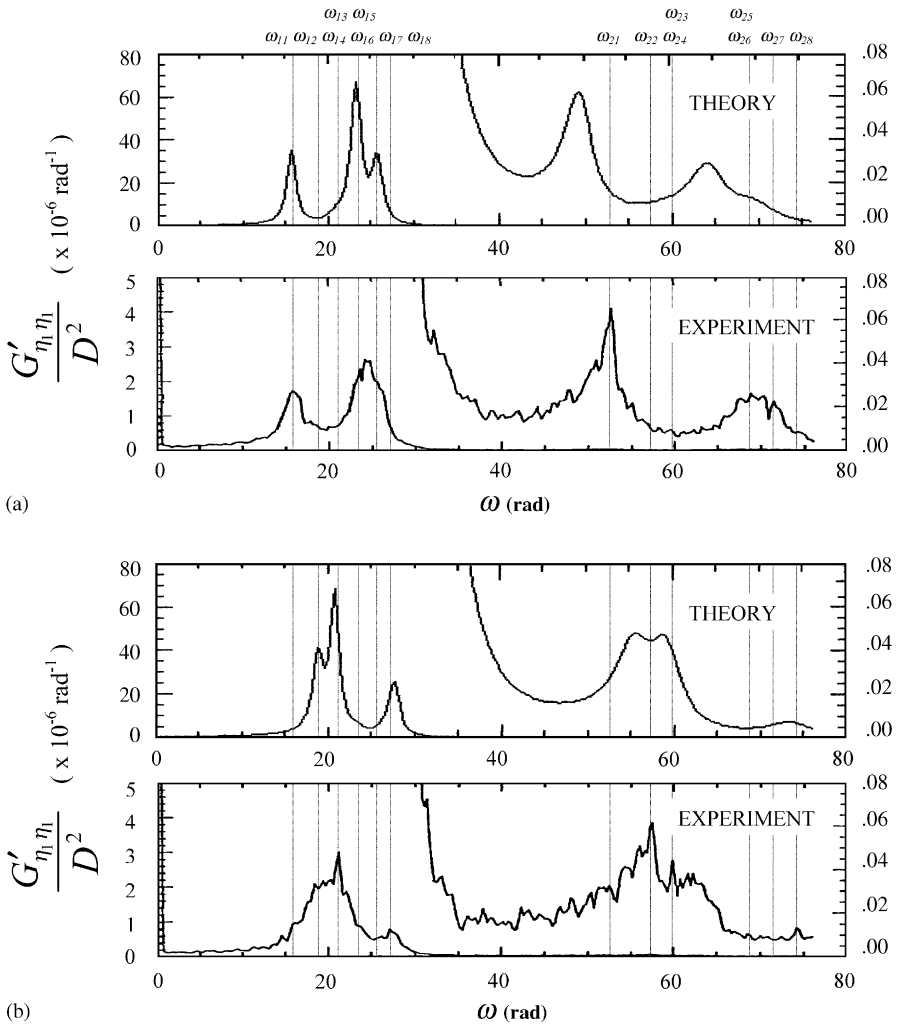

Fig. 7. Comparison of theoretical (Eq. (19a)) and experimental [16] PSDs of mid-cylinder displacements in the four-cylinder system of Fig. 6 at $u = 3.0$ in two different directions: (a) radial direction; (b) tangential direction. The frequency range spans the first and second mode frequency groups. The scales on the left ($\times 10^{-6}$) are for the first mode frequency group ($\omega_{11}, \omega_{12}, \ldots, \omega_{18}$) while those on the right (also $\times 10^{-6}$) are for the second mode group ($\omega_{21}, \omega_{22}, \ldots, \omega_{28}$). N.B.: $G'_{\eta_1\eta_1} = (\Omega/2\pi\omega)G_{\eta_1\eta_1} = (\Omega/\pi\omega)S_{\eta_1\eta_1}$ [1,10,16].

response PSDs. Eq. (20a) will offer an improvement in this regard. The other factors can be alleviated through further empirical research.

7.2. The response using Eq. (20a)

The response of the same four-cylinder system at the same flow velocity ($u = 3.0$), as in the preceding section, is calculated using Eq. (20a), for comparison with that using Eq. (19a). The differential wall-pressure PSD is in principle again given by Eq. (25); however, this time $d_0\alpha_0$ must

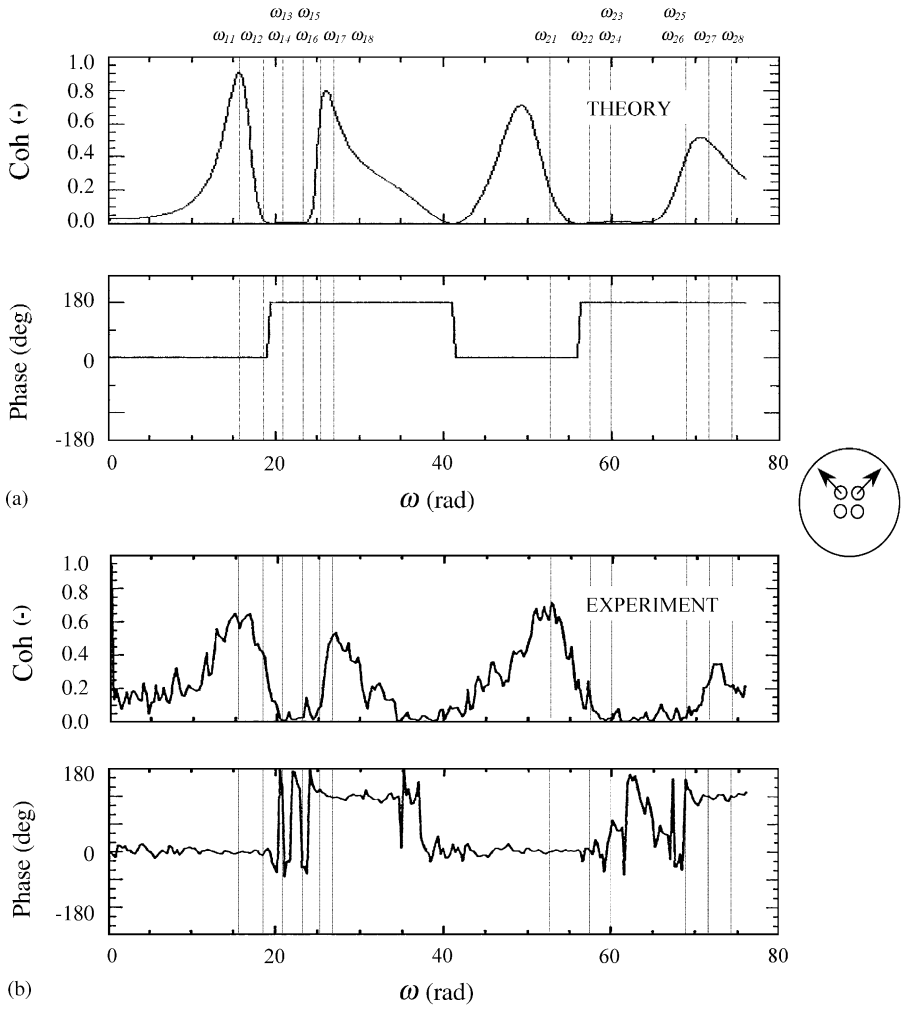

Fig. 8. Comparison of theoretical (Eq. (19a)) and experimental [16] coherences and phases between an adjacent pair of radial-direction, mid-cylinder displacements in the four-cylinder system of Fig. 6 at $u = 3.0$, corresponding to Fig. 7.

be determined for the system. This is done implicitly by utilizing an in situ measurement of $S_{\overline{pp}}(\ldots)$ at $u = 3.0$.[23] The in situ PSD (unpublished data by Gagnon) was measured at mid-longitudinal location in the "tangential" direction on one of the four cylinders in the system. In the frequency range of interest, it is given approximately by the following:

$$S_{\overline{pp}}(f) \simeq 7.5 \times 10^{-8} f \text{ kPa}^2/\text{Hz},$$
$$0 \leqslant f \leqslant 12.5 \text{ Hz or } 0 \leqslant fD_h/U \leqslant 0.76 \text{ cycles or } 0 \leqslant \omega \leqslant 76.27 \text{ rad}. \quad (28)$$

Utilizing this in Eq. (20a) the mid-cylinder response PSDs and CSDs were calculated on the computer as previously. Qualitatively, the comparison between theory and experiment is as good

[23] An in situ measurement of $S_{\overline{pp}}(\ldots)$ also corrects the $\pm 80\%$ uncertainty in b_s.

Table 4
Comparison of the major peaks (magnitudes at modal frequencies) of the experimental PSDs in Fig. 7 with theory at $u = 3.0$

	Direction 45° (radial)				Direction 135° (tangential)			
	First mode frequencies		Second mode frequencies		First mode frequencies		Second mode frequencies	
	ω_{11} ≈ 16	$\omega_{15} = \omega_{16}$ ≈ 24	ω_{21} ≈ 53	$\omega_{25} = \omega_{26}$ ≈ 68	$\omega_{13} = \omega_{14}$ ≈ 21	ω_{18} ≈ 28	ω_{22} ≈ 57	ω_{28} ≈ 74
Experiment [16]	1.8×10^{-6}	2.4×10^{-6}	6.5×10^{-8}	2.5×10^{-8}	3.0×10^{-6}	0.8×10^{-6}	6.25×10^{-8}	1.4×10^{-8}
SLFD model ($K''_{ij,\theta}$), Eq. (22a)	1.7×10^{-6}	2.2×10^{-6}	1.4×10^{-8}	0.75×10^{-8}	2.9×10^{-6}	0.4×10^{-6}	1.15×10^{-8}	0.18×10^{-8}
Empirical model ($K'_{ij,\theta}$), Eq. (20a)	3.8×10^{-6}	10.5×10^{-6}	2.75×10^{-8}	1.75×10^{-8}	9.5×10^{-6}	5.0×10^{-6}	2.6×10^{-8}	0.6×10^{-8}
Empirical model ($K_{ij,\theta}$), Eq. (19a)	35×10^{-6}	67.5×10^{-6}	6.25×10^{-8}	2.9×10^{-8}	69×10^{-6}	26×10^{-6}	4.75×10^{-8}	0.75×10^{-8}

Note: 1. The numbering system for ω_{ij} is based on there being eight theoretical frequencies in each mode group [16]. Some frequencies are repeated, e.g., $\omega_{15} = \omega_{16}$. 2. The units of ω_{ij} and the PSDs are rad and rad^{-1}, respectively.

as previously. However, this time, quantitative agreement between the theoretical and experimental response PSDs, in the important first mode group of frequencies,[24] is much better than before, as seen from the results given in Table 4. This improvement has resulted from the use of the in situ differential wall-pressure PSD (i.e., implicitly, in situ α_0 and b_s) instead of Eq. (25) as is, and the greater versatility of $K'_{ij,\theta}$ as compared to its counterpart, $K_{ij,\theta}$ (see the footnote in Section 4.3).

Based on observed margins of error in the experimental measurements of the quantities needed to calculate the theoretical response, an expected overall discrepancy factor of the order of 2.0 could be estimated.[25] Note that the values of the first-mode PSD peaks in Table 4, by the theory of Eq. (20a), are "almost" within this factor of 2.0 from the experimental first-mode peaks (discrepancy range: 2.11 to 6.25; cf. the range of 19.4–32.5 for the results via Eq. (19a)).

7.3. The response using Eq. (22a)

These last sample calculations of the four-cylinder system response make use of the SLFD scheme described in Section 5. The SLFD response is given by Eq. (22a), which requires the point

[24] The second and higher mode frequencies contribute insignificantly to the total response (see Fig. 7).

[25] The total error in the response calculation is an accumulation of errors of measurement in the PSD, LASDF, LOSDF, plus other system errors. Assume a 10% maximum error in the PSD; that in the LASDF is of the order of 30% (see Fig. 4); that in the LOSDF is taken to be the same as for the empirical differential wall-pressure CSDs (Eqs. (10a)–(10g)), i.e., 20%; assume the remaining unaccounted-for errors amount to no more than 20%; finally, assume the overall error is not very different from, or at least not smaller than, the average term-by-term error in the multiple summations in Eqs. (19a), (20a) and (22a) (this effectively establishes a lower bound for the expected error). Given these values and assumptions, the overall error ratio is expected to be no better than $1.10(PSD) \times 1.30(LASDF) \times 1.20(LOSDF) \times 1.20(\text{other system errors}) = 2.1$.

pressure PSD, $S_{pp}(f)$. This is taken to be one-half the in situ differential pressure PSD given earlier by Eq. (28).[26]

The mid-cylinder response PSDs and CSDs calculated on this basis, were again qualitatively very similar to Figs. 7 and 8, the only significant differences occurring in the magnitudes of the PSDs. Values of these, at the natural frequencies of the system, are given in Table 4, where comparisons are made to the results of the empirical schemes used earlier, as well as experimental measurements [16]. In the table it can be seen that the SLFD scheme compares better with experiment than do any of the empirical schemes at the first mode frequencies. It is plausible that this has occurred mainly for one or all of the following four reasons: (1) a judicious choice of the tangential direction in which to obtain an approximation for $S_{pp}(f)$ (see previous footnote); (2) the fact that the four-cylinder system is sparsely populated (Fig. 6) compared to the fully populated eight-cylinder bundle (Fig. 2) from which $K_{ij,\theta}$ and $K'_{ij,\theta}$ were obtained; the sparse four-cylinder system more closely "resembles" pipe- and annular-flow systems, with respect to $K''_{ij,\theta}$, than does the fully populated system, i.e., they have more "similar" values of D/D_h; thus, $K''_{ij,\theta}$ would appear to have been more "reasonable" for this four-cylinder system than $K'_{ij,\theta}$ or $K_{ij,\theta}$; (3) there is a closer match of Re between the excitation in the SLFD theory and the experimental four-cylinder system than in the previous two samples; and finally (4) the inclusion of the inter-cylinder wall-pressure excitation CSDs in the SLFD model, however small, may have had a small but substantial, cumulative effect on the result [1]. More research should be done to investigate these matters further.

Finally, small discrepancies still remaining between theory and experiment can probably be attributed in part to non-linear effects such as those excluded by the quasi-static assumption for the excitation forces on the walls of the vibrating cylinders, in part to uncharacterized fluid flow excitation in the developing part of the flow and in part to other limitations of the model [16].

8. Comparative computations of cylinder response spectra utilizing the full and reduced stochastic equations

Shown in Table 5 are the times-of-computation ratios for the sample calculations of normalized response spectra [defined in Eqs. (19a) and (22a)] using the full and reduced equations presented in Section 2. The results show that significant savings can be achieved with the reduced equations (4)–(7), compared to using the full equation (3); e.g., from the table, the calculation of the response PSD by the SLFD correlation scheme of Section 5 with three comparison functions

[26] This is valid since, in the tangential direction of Fig. 6, the diametrically correlated components of the differential pressure balance each other (by geometric symmetry), leaving only the uncorrelated components to contribute to cylinder vibration, and the PSDs of the uncorrelated components are equal in magnitude (again by symmetry). Specifically, if p_1 and p_2 are the uncorrelated components of pressure, then

$$G_{\overline{pp}} = (G_{p_1p_1} + G_{p_2p_2}) - (G_{p_1p_2} + G_{p_2p_1}) = 2G_{p_1p_1},$$

since $G_{p_1p_1} = G_{p_2p_2}$ (by symmetry) and $G_{p_1p_2} = G_{p_2p_1} = 0$ (uncorrelated). Note from Fig. 6 that the cross-sectional geometry, while symmetric in the tangential direction, is not in others. Thus, the above may not be true in other directions. Note, however, that it is true in all directions in a fully populated rectangular array of cylinders (see Appendix B). The use of the tangential direction PSD in this example should therefore be viewed as a good approximation for the "laterally homogeneous" $S_{pp}(f)$ in Eq. (22a).

Table 5
"Times-of-computation" ratios— Eq. (3): Eq. y (for $K = 4$, $N = 3$)[a] for normalized response spectra

		Eq. y			
		(4)	(5a)	(6a)[b]	(7)[b]
SLFD correlation scheme (*see Section* 5.2)					
Eq. (3)[c]	(PSD Only)	2.26:1	41.36:1	35.02:1	186.76:1
	(PSD + CSD)	3.89:1	97.23:1	n/a	n/a
	(CSD Only)	6.78:1	475.59:1	n/a	n/a
Empirical correlation scheme (*see Section* 4.2)					
Eq. (3)[c]	(PSD only)	1.87:1	26.23:1	26.23:1	96.17:1
	(PSD + CSD)	2.61:1	55.71:1	n/a	n/a
	(CSD only)	3.39:1	163.83:1	n/a	n/a

A CSD calculation consists of the inter-cylinder spectral densities in the Cartesian directions (i.e., $S_{z_1z_2}$, $S_{y_1y_2}$, $S_{z_1y_2}$ and $S_{y_1z_2}$) needed to calculate the inter-cylinder response CSDs of two pairs of cylinders in arbitrary polar directions [e.g., pairs (1, 2) and (1, 3)].

[a] $N = 1$ for Eqs. (5a) and (7)—see Table 1.

[b] Eqs. (6a) and (7) are single-cylinder equations and cannot determine inter-cylinder response CSDs.

[c] A PSD calculation consists of the same-cylinder spectral densities in the Cartesian directions (i.e., S_{zz}, S_{yy}, and S_{zy}) needed to calculate the response PSD of a cylinder in an arbitrary polar direction.

($N = 3$), using Eq. (3), the full equation, took 2.26 times as long as it did using Eq. (4), the NOINTEC reduced equation, and 41.36 times as long as it did using Eq. (5a), the NOINTEC 1 reduced equation.

9. Conclusions

In the foregoing, stochastic equations of varying degrees of computational complexity and efficiency for determining the random vibratory response of cylindrical structures have been given, with application to cylinders subjected to turbulent axial flow. Analytical approximations for the lateral fluid forcing functions have been presented, based on previous wall-pressure measurements in a particular bundle of cylinders configured cross-sectionally in a square-array pattern and a few other results pertaining to other set-ups from the literature [3,6–8,16–22,26]. The model of the excitation derived from these approximations was obtained for $6800 \leqslant Re \leqslant 48\,000$ and $D/D_h = 2.095$.

The generality of the present or any other similar force-field approximations for arbitrary bundle configurations and test rigs remains to be more thoroughly investigated. Possible tools for this kind of investigation include turbulence correlation length scales [6]. Also, it is to be emphasized that the present data and all its implications strictly apply to excitation frequencies above fD_h/U of the order of 0.25. This resulted because of the absence of empirical data below that point [3,6]. For the purpose of making sample calculations, certain logical assumptions (the zero-frequency/zero-PSD assumption and a linear-descent- to-zero assumption) were necessary in the region between $fD_h/U = 0.0$ and 0.25. The zero-frequency/zero-PSD assumption is based on

the fact that it can be accurately inferred that under the condition of balanced static pressure the excitation PSD (of differential pressure), hence the CSD, is exactly zero at zero frequency, i.e., at the static condition. The need for the second assumption, the linear approximation between $fD_h/U = 0$ and 0.25, shows that more research is needed to determine the exact behaviour of the phenomenon near "static" conditions—although, this gap being small, the error introduced by a linear assumption would be minimal.

All in all, the present empirical approximations for characterization of the turbulent force field on stationary cylinders may be summarized as follows. Indications are that the force field depends fundamentally upon the following correlation parameters and functions: b_s, a "quietness" function of proportionality (called a bundle system "constant"); c, a confinement function; β, γ, lateral and longitudinal correlation decay functions, respectively; d, a pressure-field development function; α, a wall-pressure PSD shape and azimuthal distribution function; P, a Reynolds-number-dependent power function; $\bar{U}_c$, average wall-pressure disturbance convection velocity; $K_{ij,\theta}$, lateral spectral density factors (LASDF), and $K_{\ell n,x}$, longitudinal spectral density factors (LOSDF).

These have been discussed in detail here and elsewhere in the literature [3,6,10,16,26]. Excluding d, they have all been determined only in the fully developed part of the flow of the eight-cylinder bundle mentioned in this paper [3,6]. More research needs to be conducted in the developing part of the flow in this, as well as other, bundle configurations. Also, wider ranges of Re and D/D_h need to be investigated.

The excitation CSD can be approximated by the product of the excitation PSD and lateral and longitudinal correlation functions or factors as shown in Appendix D. By the reasoning of Appendix D, this approximation will probably be more accurate for low frequencies and small separation distances than for higher frequencies and larger separation distances. Fortunately, the correlations tend to be insignificantly small at the higher frequencies and larger separation distances, while most of the vibration occurs only at the lower frequencies. The separation of planes into lateral and longitudinal parts is based on Corcos' model of the turbulent wall-pressure field [32], and has been used successfully in previous studies of this kind [1,7,8,16,23,24,27]. Subsequent analysis gives rise to the lateral and longitudinal spectral density factors as has been discussed. The longitudinal spectral density factors involve double integrals over the lengths of the cylinders, a summary of which, using complex variables and the Euler Bernoulli beam eigenfunctions, is given in Appendix C for arbitrary cylinder boundary conditions.

Sample calculations were conducted for the response of a four-cylinder system using the equations presented in this paper and the "quasi-static" excitation force-per-unit-length CSDs that were developed. The theoretical results were compared to experimental results for the same system found in the literature [16]. Those by Eq. (20a) compared much better with experiment than those by Eq. (19a), showing the advantage of $K'_{ij,\theta}$ (normalized LASDF) over $K_{ij,\theta}$ (unnormalized LASDF) in this case, both of which were determined from measurements of the wall-pressure field in the eight-cylinder stationary bundle. The dependency of the former, $K'_{ij,\theta}$, on the eight-cylinder wall-pressure PSD shape function, α_0, was removed through division or "normalization" by α_0, making it more applicable to the four-cylinder bundle, which was inherently (by reason of a different geometry) under the influence of a different wall-pressure PSD shape function. In short, $K'_{ij,\theta}$ was more "transferable" in this example from one bundle configuration to the other, than $K_{ij,\theta}$; hence better results were obtained using $K'_{ij,\theta}$. Additionally,

the in situ wall-pressure PSD used in Eq. (20a) avoided estimation errors in b_s. This also helped to improve the results. An in situ PSD can be used in conjunction with Eq. (9b) in a given rig to minimize the amount of wall-pressure PSD measurements necessary in the rig.

For comparison purposes, sample calculations involving $K''_{ij,\theta}$, i.e., the SLFD scheme given by Eq. (22a), were also made. Results agreed with experiment even better than those using $K'_{ij,\theta}$, for the same four-cylinder system. Four possible explanations for this were given. First, the four-cylinder system, with its greater regions of "open space", more closely "resembles" the pipe- and annular-flow systems upon which the SLFD correlation scheme is based (i.e., they have "similar" D/D_h), than does the more densely populated 8-cylinder system from which $K_{ij,\theta}$ and $K'_{ij,\theta}$ were determined. Second, the improved agreement between theory and experiment could be due in part to the cumulative effects of inter-cylinder wall-pressure excitation CSDs, however small, and their inclusion in the SLFD model [1]. Third, the choice of the tangential direction wall-pressure PSD, and not any other direction PSD, to approximate $S_{pp}(f)$ in Eq. (22a) could also have favourably impacted on the results. Fourth and last, the range of Re over which the SLFD correlation scheme was obtained contains the Re at which the experimental four-cylinder response was measured and therefore it is probably more valid for the four-cylinder system than the empirical schemes involving $K_{ij,\theta}$ and $K'_{ij,\theta}$ which were obtained at much lower Re.

More research is needed to resolve and further explain these matters. The effect of cylinder motion on the excitation force field should also be researched, so that larger-amplitude vibrations could be studied (i.e., higher flow velocities). Moreover, the analytical characterization of the wall-pressure excitation will benefit greatly from research into the structure of wall-bounded turbulent flow [33].

Finally, this paper also shows that significant savings, in terms of computational efficiency, can be achieved when computing the cylinder response spectra by utilizing simplified or reduced versions of the full equation for cylinder vibration in a bundle of cylinders. This has implications for value-engineering design of large systems based on differing cylinder bundle configurations.

Acknowledgements

This work was accomplished with financial assistance from the Natural Sciences and Engineering Research Council of Canada and Le Programme FCAR du Québec.

Appendix A. Derivation of Eqs. (3)–(5)

A.1. Eq. (3)

The displacement vector, $\boldsymbol{\eta}(x,t)$ (Eq. (2)) is expanded in a series of Galerkin comparison functions,

$$\boldsymbol{\eta}(x,t) = \sum_{n=1}^{N} \phi_n(x)\mathbf{q}_n(t), \tag{A.1}$$

where $\phi_n(x)$ are the comparison functions satisfying the boundary conditions of the problem and $\mathbf{q}_n = \{q_{n_1}, q_{n_2}, \ldots, q_{n_{2K}}\}^{\mathrm{T}}$, the nth generalized vector corresponding to the displacement vector, $\boldsymbol{\eta} = \{\eta_1, \eta_2, \ldots, \eta_{2K}\}^{\mathrm{T}}$.

Eq. (1) is then written as

$$\sum_{n=1}^{N} [\mathbf{M}(x)\phi_n(x)\ddot{\mathbf{q}}_n(t) + \mathbf{C}(x)\phi_n(x)\dot{\mathbf{q}}_n(t) + \mathbf{K}(x)\phi_n(x)\mathbf{q}_n(t)] = \mathbf{f}(x,t), \tag{A.2}$$

where $\mathbf{f}(x,t) = \{\mathbf{f}_z(x,t), \mathbf{f}_y(x,t)\}^{\mathrm{T}}$.

Multiplying by the weighting function, $W_{n'}(x)$, and integrating over x to eliminate the space variable, this becomes

$$\sum_{n=1}^{N} \int_0^L [W_{n'}(x)\mathbf{M}(x)\phi_n(x)\ddot{\mathbf{q}}_n(t) + W_{n'}(x)\mathbf{C}(x)\phi_n(x)\dot{\mathbf{q}}_n(t) + W_{n'}(x)\mathbf{K}(x)\phi_n(x)\mathbf{q}_n(t)]\,dx$$
$$= \int_0^L W_{n'}(x)\mathbf{f}(x,t)\,\mathrm{d}x, \quad n' = 1, 2, \ldots, N, \tag{A.3a}$$

or in matrix form

$$[M]\ddot{\mathbf{q}} + [C]\dot{\mathbf{q}} + [K]\mathbf{q} = \mathbf{f}(t), \tag{A.3b}$$

where

$$[M] = \begin{bmatrix} [m_{1'1}] & [m_{1'2}] & \ldots & [m_{1'N}] \\ [m_{2'1}] & [m_{2'2}] & \ldots & [m_{2'N}] \\ \vdots & \vdots & & \vdots \\ [m_{N'1}] & [m_{N'2}] & \ldots & [m_{N'N}] \end{bmatrix}, \quad [m_{n'n}] = \int_0^L W_{n'}\mathbf{M}\phi_n\,\mathrm{d}x, \tag{A.3c}$$

$$[C] = \begin{bmatrix} [c_{1'1}] & [c_{1'2}] & \ldots & [c_{1'N}] \\ [c_{2'1}] & [c_{2'2}] & \ldots & [c_{2'N}] \\ \vdots & \vdots & & \vdots \\ [c_{N'1}] & [c_{N'2}] & \ldots & [c_{N'N}] \end{bmatrix}, \quad [c_{n'n}] = \int_0^L W_{n'}\mathbf{C}\phi_n\,\mathrm{d}x, \tag{A.3d}$$

$$[K] = \begin{bmatrix} [k_{1'1}] & [k_{1'2}] & \ldots & [k_{1'N}] \\ [k_{2'1}] & [k_{2'2}] & \ldots & [k_{2'N}] \\ \vdots & \vdots & & \vdots \\ [k_{N'1}] & [k_{N'2}] & \ldots & [k_{N'N}] \end{bmatrix}, \quad [k_{n'n}] = \int_0^L W_{n'}\mathbf{K}\phi_n\,\mathrm{d}x, \tag{A.3e}$$

$$\mathbf{q} = \{\mathbf{q}_1, \mathbf{q}_2, \ldots, \mathbf{q}_n\}^{\mathrm{T}} \tag{A.3f}$$

and

$$\mathbf{f}(t) = \int_0^L \{W_1\mathbf{f}(x,t), W_2\mathbf{f}(x,t), \ldots, W_N\mathbf{f}(x,t)\}^{\mathrm{T}}\,\mathrm{d}x. \tag{A.3g}$$

Taking the finite Fourier transform of Eq. (A.3b) and retaining only the steady state producing terms yields [see Eqs. (A.10a) and (10b)]

$$[-\Omega^2[M] + \mathrm{i}\Omega[C] + [K]]\mathbf{Q}(\Omega, T) = \mathbf{F}(\Omega, T), \tag{A.4a}$$

where

$$\mathbf{Q}(\Omega, T) = \int_0^T \mathbf{q}(t)\mathrm{e}^{-\mathrm{i}\Omega t}\,\mathrm{d}t, \tag{A.4b}$$

$$\mathbf{F}(\Omega, T) = \int_0^T \mathbf{f}(t)\mathrm{e}^{-\mathrm{i}\Omega t}\,\mathrm{d}t. \tag{A.4c}$$

Solving (A.4a),

$$\mathbf{Q}(\Omega, T) = [H(\Omega)]\mathbf{F}(\Omega, T), \tag{A.5a}$$

where the frequency response function matrix is defined as

$$[H(\Omega)] = [-\Omega^2[M] + \mathrm{i}\Omega[C] + [K]]^{-1}. \tag{A.5b}$$

Considering each element of $\mathbf{Q}(\Omega, T)$ more explicitly (using also Eqs. (A.4b), (A.4c) and (A.3g)),

$$\begin{aligned} Q_\beta(\Omega, T) &= \sum_{q=1}^{2KN} H_{\beta q}(\Omega)\mathscr{F}_q(\Omega, T) \\ &= \sum_{q=1}^{2KN} H_{\beta q}(\Omega) \int_0^L W_{a(q)}(x)F_{b(q)}(x, \Omega, T)\,\mathrm{d}x, \end{aligned} \tag{A.5c}$$

where

$$F_{b(q)}(x, \Omega, T) = \int_0^T f_{b(q)}(x, t)\,\mathrm{e}^{-\mathrm{i}\Omega t}\,\mathrm{d}t, \quad f_{b(q)}(x, t) \text{ being the element of } \mathbf{f}(x, t), \tag{A.5d}$$

$$a(q) = \text{largest integer} \leqslant \{(2K + q - 1)/2K\}, \quad \text{changing from 1 to } N \text{ as } q \text{ goes from 1 to } 2KN, \tag{A.5e}$$

$$b(q) = q - 2K[a(q) - 1], \quad \text{cycling repeatedly from 1 to } 2K \text{ as } q \text{ goes from 1 to } 2KN. \tag{A.5f}$$

Rewriting Eq. (A.1) in elemental form,

$$\eta_j(x, t) = \sum_{n=1}^{N} \phi_n(x)q_n^j(t). \tag{A.6}$$

Taking the finite Fourier transform of this gives

$$\aleph_j(x, \Omega, T) = \sum_{n=1}^{N} \phi_n(x)Q_n^j(\Omega, T), \tag{A.7a}$$

where

$$\aleph_j(x,\Omega,T)=\int_0^T \eta_j(x,t)\,\mathrm{e}^{-\mathrm{i}\Omega t}\,\mathrm{d}t, \tag{A.7b}$$

$$Q_n^j(\Omega,T)=\int_0^T q_n^j(t)\,\mathrm{e}^{-\mathrm{i}\Omega t}\,\mathrm{d}t. \tag{A.7c}$$

From the definition of $\mathbf{q}_n(t)$ in Eq. (A.1) and $\mathbf{q}$ in Eq. (A.3f), we can write

$$Q_n^j(\Omega,T)=Q_{\beta(n,j)}(\Omega,T), \tag{A.8a}$$

where

$$\beta(n,j)=2K(n-1)+j. \tag{A.8b}$$

Substituting for $Q_n^j(\Omega,T)$ in Eq. (A.7a), using Eqs. (A.8a), (A.8b) and (A.5c), gives

$$\aleph_j(x,\Omega,T)=\sum_{n=1}^{N}\phi_n(x)\sum_{q=1}^{2KN}H_{\beta(n,j),q}(\Omega)\int_0^L W_{a(q)}(x_1)F_{b(q)}(x_1,\Omega,T)\,\mathrm{d}x_1. \tag{A.9}$$

The response and excitation CSDs are now defined as [9]

$$S_{\eta_i\eta_j}(x,x',\Omega)=\lim_{T\to\infty}\frac{1}{T}\aleph_i^*(x,\Omega,T)\aleph_j(x',\Omega,T), \tag{A.10a}$$

$$S_{f_{b(p)}f_{b(q)}}(x_1,x_2,\Omega)=\lim_{T\to\infty}\frac{1}{T}F_{b(p)}^*(x_1,\Omega,T)F_{b(q)}(x_2,\Omega,T) \tag{A.10b}$$

with the corresponding cross-correlations,

$$R_{\eta_i\eta_j}(x,x',\bar{t})=\frac{1}{2\pi}\int_{-\infty}^{\infty}S_{\eta_i\eta_j}(x,x',\Omega)\mathrm{e}^{\mathrm{i}\Omega\bar{t}}\,\mathrm{d}\Omega, \tag{A.10c}$$

$$R_{f_{b(p)}f_{b(q)}}(x_1,x_2,\bar{t})=\frac{1}{2\pi}\int_{-\infty}^{\infty}S_{f_{b(p)}f_{b(q)}}(x_1,x_2,\Omega)\mathrm{e}^{\mathrm{i}\Omega\bar{t}}\,\mathrm{d}\Omega. \tag{A.10d}$$

Then, by substituting Eq. (A.9) into Eq. (A.10a) and applying Eq. (A.10b), Eq. (3) of the main text is obtained, having $W(x)=\phi(x)$.

A.2. Eq. (4)

Eq. (4) follows from Eq. (3) when

$$\begin{aligned} S_{f_{b(p)}f_{b(q)}}(x_1,x_2,\Omega)=0, \quad & b(p)\neq b(q) \text{ or } b(q)+K \text{ when } b(q)\leqslant K,\\ & b(p)\neq b(q) \text{ or } b(q)-K, \text{ when } b(q)>K. \end{aligned} \tag{A.11}$$

This can be demonstrated by considering the components (or elements) of the generalized force-per-unit-length CSD matrix that are non-zero according to the above condition. The indices (or subscripts) q and n in Eq. (3) may then be redefined as the new subscripts q' and n' given in Eq. (4) in order to accommodate or include those non-zero components and exclude these [Eq. (A.11)] that are zero. The range of n' must then be 1 to $2N$ to include all N modes in the two directions z and y as indicated in Eq. (4).

A.3. Eq. (5)

Eq. (5a) follows from Eq. (4) when $N = 1$.

Appendix B. Properties of force-per-unit-length and cylinder displacement PSDs and CSDs for an infinite square array based on geometric symmetry

The following Theorems 1–3, apply to cylinder vectors in general, i.e., to forces as well as displacements.

Theorem 1. *The PSD is the same all around a cylinder in a given lateral plane.*

Proof. See Fig. 9. By symmetry

$$G_{f_{y'}f_{y'}} = G_{f_{z'}f_{z'}}, \quad G_{f_{y'}f_{z'}} = -G_{f_{y'}f_{z'}} = 0$$

and

$$G_{f_{z'}f_{y'}} = -G_{f_{z'}f_{y'}} = 0.$$

Also by resolving vectors in the direction ϕ,

$$f_\phi = f_{z'} \cos\phi + f_{y'} \sin\phi.$$

Therefore,

$$\begin{aligned} G_{f_\phi f_\phi} &= G_{f_{z'}f_{z'}} \cos^2\phi + (G_{f_{z'}f_{y'}} + G_{f_{y'}f_{z'}}) \cos\phi \sin\phi + G_{f_{y'}f_{y'}} \sin^2\phi \\ &= G_{f_{z'}f_{z'}} = G_{f_{y'}f_{y'}} \quad \text{for all } \phi. \end{aligned}$$

Theorem 2. *The inter-cylinder CSDs between the z and y directions shown are zero in a given lateral plane.*

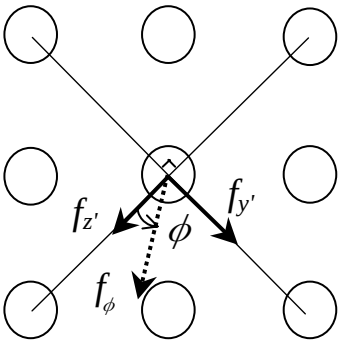

Fig. 9. Diagram used in the proof of Theorem 1 of Appendix B.

Proof. See Fig. 10. By symmetry,

$$G_{f_{z_1}f_{y_2}} = G_{f_{z_1}(-f_{y_2})} = -G_{f_{z_1}f_{y_2}} = 0, \quad G_{f_{z_2}f_{y_1}} = G_{f_{z_2}(-f_{y_1})} = -G_{f_{z_2}f_{y_1}} = 0.$$

Theorem 3. *CSDs between any two orthogonal directions on a given cylinder are imaginary* (*real parts are zero*) *in a given lateral plane.*

Proof. See Fig. 11. By symmetry,

$$G_{ab} = G_{bc} = G_{cd} = G_{da}.$$

However, $G_{da} = -G_{ba} = -G_{ab}^*$; therefore $G_{ab} = -G_{ab}^*$, and the real part of G_{ab} must be zero, i.e., G_{ab} is imaginary, for all rotations θ.

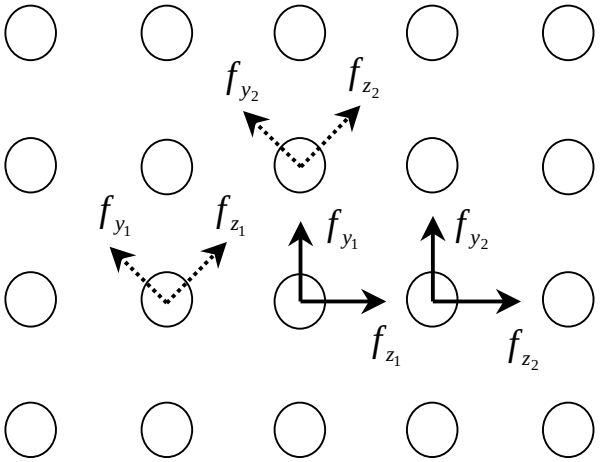

Fig. 10. Diagram used in the proof of Theorem 2 of Appendix B.

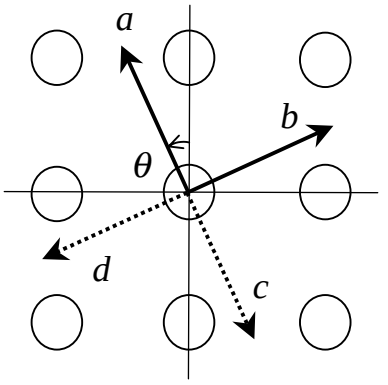

Fig. 11. Diagram used in the proof of Theorem 3 of Appendix B.

Appendix C. Evaluation of LOSDF

This appendix summarizes the development in Ref. [10]. LOSDF, the longitudinal spectral density factors, in the differential (empirical) and point (SLFD) wall pressure correlation schemes are given by Eqs. (19b) and (22c), respectively. As stated before, the two equations are very similar, in fact almost identical, in form. The only difference in form occurs in the choice of flow velocity to define the reduced frequency (or Strouhal number) in the function γ; the first uses bulk flow velocity U in γ, while the second utilizes the convection flow velocity, $\bar{U}_c$. The importance, or net effect, of this is that the method of evaluation of both double integrals, i.e., both equations, is exactly the same. Hence it need only be demonstrated from one of them.

Accordingly, Eq. (19b) can be rewritten as follows:

$$K_{\ell n,x}\left(\frac{fD_h}{U},\ldots\right)=L^2\int_0^1 \mathrm{d}\xi_1\int_0^1 \mathrm{d}\xi_2\,\phi_\ell(\xi_1)\phi_n(\xi_2)\exp\left(-b\frac{fL}{U}|\bar{\xi}|\right)\exp\left(-\mathrm{i}\frac{2\pi fL}{aU}\bar{\xi}\right),\quad \ell,n=1,2,\ldots,N, \tag{C.1}$$

where $\xi=x/L$, $\bar{\xi}=\xi_2-\xi_1$, $b=0.7$, and γ has been substituted by Eq. (10c) in the direction $\phi_s=0^\circ$. The comparison (or weighting) functions, $\phi_\ell(\xi)$ and $\phi_n(\xi)$, in the solution of the problem, have been chosen as the orthonormal Euler–Bernoulli beam eigenfunctions that satisfy the boundary conditions of the problem (e.g., for pinned–pinned cylinders, choose $\phi_\ell(\xi)=\sqrt{2}\sin\ell\pi\xi$). Then, noting that $\mathrm{d}^4\phi_\ell(\xi)/\mathrm{d}\xi^4=\lambda_\ell^4\phi_\ell(\xi)$, where λ_ℓ ($\ell=1,2,\ldots,N$) are the beam eigenvalues (for pinned–pinned conditions, $\lambda_\ell=\ell\pi$), Eq. (C.1) can be integrated by parts repeatedly, for the case of $fL/U>0.0$, to yield [10]

$$\begin{aligned}K_{\ell n,x}(fD_h/U,\ldots)/L^2=&-A(-z^*,\ell,n)-I(z^*,n,0.0)\times B(-z^*,\ell,n)+A(z,\ell,n)\\&+\mathrm{e}^{-z}I(-z,n,1.0)\times B(z,\ell,n),\quad \ell,n=1,2,\ldots,N,\end{aligned} \tag{C.2a}$$

where

$$z=\frac{fL}{U}\left(b+\mathrm{i}\frac{2\pi}{a}\right),\quad \mathrm{i}=\sqrt{-1}, \tag{C.2b}$$

$$A(z,\ell,n)=\frac{1}{1-\lambda_n^4/z^4}\left\{\frac{a_{\ell n}}{z}+\frac{b_{\ell n}}{z^2}+\frac{c_{\ell n}}{z^3}+\frac{f_{\ell n}}{z^4}\right\}, \tag{C.2c}$$

$$I(z,n,\xi)=\frac{\phi_n(\xi)}{z}-\frac{1}{z^2}\frac{\mathrm{d}\phi_n(\xi)}{\mathrm{d}\xi}+\frac{1}{z^3}\frac{\mathrm{d}^2\phi_n(\xi)}{\mathrm{d}\xi^2}-\frac{1}{z^4}\frac{\mathrm{d}^3\phi_n(\xi)}{\mathrm{d}\xi^3} \tag{C.2d}$$

and

$$B(z,\ell,n)=\frac{1}{(1-\lambda_\ell^4/z^4)}\frac{1}{(1-\lambda_n^4/z^4)}\{\mathrm{e}^z I(z,\ell,1.0)-I(z,\ell,0.0)\}. \tag{C.2e}$$

In Eq. (C.2c), $a_{\ell n}$ through $f_{\ell n}$ are the weighted residuals given by the following:

$$a_{\ell n} = \int_0^1 \phi_\ell(\xi)\phi_n(\xi)\,\mathrm{d}\xi, \quad b_{\ell n} = \int_0^1 \phi_\ell(\xi)\frac{\mathrm{d}\phi_n(\xi)}{\mathrm{d}\xi}\,\mathrm{d}\xi,$$
$$c_{\ell n} = \int_0^1 \phi_\ell(\xi)\frac{\mathrm{d}^2\phi_n(\xi)}{\mathrm{d}\xi^2}\,\mathrm{d}\xi, \quad f_{\ell n} = \int_0^1 \phi_\ell(\xi)\frac{\mathrm{d}^3\phi_n(\xi)}{\mathrm{d}\xi^3}\,\mathrm{d}\xi. \tag{C.2f}$$

For the case where $fL/U = 0$, Eq. (C.1) simplifies to

$$K_{\ell n,x}(fD_h/U, \ldots)/L^2 = \int_0^1 \mathrm{d}\xi_1 \int_0^1 \mathrm{d}\xi_2\, \phi_\ell(\xi_1)\phi_n(\xi_2). \tag{C.2g}$$

(For the orthonormal pinned–pinned boundary conditions, this equals zero when either ℓ or n is even, and $8/(\ell n\pi^2)$ when both ℓ and n are odd.)

Appendix D. Exact relations which aid the characterization of wall-pressure and force-per-unit-length CSDs

D.1. Wall-pressure CSDs

It can be shown that, in terms of an intermediary pressure, p_2, the CSD between pressures, p_1 and p_3, can be written as

$$S_{p_1p_3} = \frac{S_{p_1p_2}S_{p_2p_3}}{S_{\hat{p}_2\hat{p}_2}}, \tag{D.1}$$

where $\hat{p}_2$ is the component of p_2 that is correlated with both p_1 and p_3 (see Fig. 12).[27] The methodology for proving Eq. (D.1) can be found in Ref. [26]. The proof is produced here and goes as follows. Assume that the pressures p_1, p_2 and p_3 each consist of two components only, which are: (a) completely intercorrelated components, $\hat{p}_1$, $\hat{p}_2$ and $\hat{p}_3$, respectively, and (b) completely uncorrelated or noise components, n_1, n_2 and n_3, respectively.[28] Letting capital letters represent

[27] It can be shown [26] that $S_{\hat{p}_2\hat{p}_2} = S_{p_2p_2}[\gamma^2_{p_1p_2}\gamma^2_{p_2p_3}/\gamma^2_{p_1p_3}]^{1/2}$ where $\gamma^2_{p_ip_j} = |S_{p_ip_j}|^2/(S_{p_ip_i}S_{p_jp_j})$, the coherence between p_i and p_j; $i,j = 1,2,3$. It would appear that knowing this is of no practical value, other than possibly to validate Eq. (D.1) experimentally, since the measurement of $\gamma^2_{p_1p_3}$ requires the knowledge of $S_{p_1p_3}$ a priori, which is the quantity initially sought.

[28] By analogy with $\hat{p}_2$ defined in Eq. (D.1), $\hat{p}_1$ is that component of p_1 that correlates with both p_2 and p_3, and similarly, $\hat{p}_3$, the component of p_3 that correlates with both p_1 and p_2. It is unlikely that in the turbulent pressure field of a cylinder bundle, significant partially correlated components of p_2 would exist, i.e., it is unlikely that when p_1 correlates with p_3, some part of p_2 will also correlate significantly with p_3 but not with p_1, or with p_1 but not with p_3 (see Fig. 12). This is because the high-frequency components of correlated pressure (the small eddy formations) correlate over shorter distances than the low-frequency components (the larger eddy formations) and their correlation, over the same distance, is also smaller in magnitude than those of the larger, low-frequency eddies (this can be deduced from the fact that the correlation decay functions, β and γ decrease relatively rapidly with frequency and separation distance, i.e., with $fL_{\min}(\theta_r,\theta_s)/\bar{U}_c$ and $f\bar{x}/\bar{U}_c$—see Eqs. (21b) and (21c) and see also Refs. [3,8,18,19,26,29]). Thus, the partially correlated components of p_2 consist mainly of the small, high-frequency eddy formations and can be neglected in comparison to the larger, low-frequency ones [26].

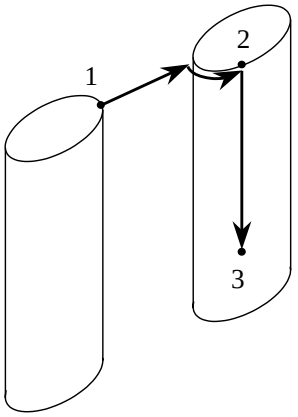

Fig. 12. Diagram used to obtain the CSD of the pressures at two arbitrary points on two adjacent cylinders.

finite Fourier transforms of the lower case letters, the right-hand side of (D.1) can be written as

$$\frac{S_{p_1p_2}S_{p_2p_3}}{S_{\hat{p}_2\hat{p}_2}} = \frac{\lim_{T\to\infty}(1/T)(\hat{P}_1^* + N_1^*)(\hat{P}_2 + N_2)\lim_{T\to\infty}(1/T)(\hat{P}_2^* + N_2^*)(\hat{P}_3 + N_3)}{\lim_{T\to\infty}(1/T)(\hat{P}_2^*\hat{P}_2)}, \quad \text{(D.2)}$$

where T is the finite time span of the signals, p_1, etc., under the Fourier transforms. Noting that the product of the limits is the limit of the product when the product exists, and that all products involving noise components, N_1, N_2 and N_3, vanish as T tends to infinity, the above simplifies to

$$\frac{S_{p_1p_2}S_{p_2p_3}}{S_{\hat{p}_2\hat{p}_2}} = \lim_{T\to\infty}\frac{1}{T}(\hat{P}_1^*\hat{P}_3) = S_{p_1p_3}, \quad \text{(D.3)}$$

which is Eq. (D.1).

Now, by multiplying and dividing Eq. (D.1) throughout by $[S_{p_1p_1}S_{p_3p_3}]^{1/2}$, it can be rewritten as

$$S_{p_1p_3} = [S_{p_1p_1}S_{p_3p_3}]^{1/2}\Psi_{p_1\hat{p}_2}\Psi_{\hat{p}_2p_3}, \quad \text{(D.4a)}$$

where

$$\Psi_{p_1\hat{p}_2} = \frac{S_{p_1p_2}}{[S_{p_1p_1}S_{\hat{p}_2\hat{p}_2}]^{1/2}}, \quad \text{(D.4b)}$$

$$\Psi_{\hat{p}_2p_3} = \frac{S_{p_2p_3}}{[S_{\hat{p}_2\hat{p}_2}S_{p_3p_3}]^{1/2}}. \quad \text{(D.4c)}$$

Eqs. (D.4a)–(D.4c) are all exact relations which can be used to guide the characterization of wall pressure CSDs in a bundle of cylinders. Thus, comparing Eq. (D.4a) to Eq. (9a) in the main text, noting Eqs. (D.4b) and (D.4c) above, and assuming $S_{p_2p_2}$ can be used to approximate $S_{\hat{p}_2\hat{p}_2}$, the

following associations can be made:

$$S_{p_1p_3} \to S_{\bar{p}_r\bar{p}_s}(\ldots), \quad S_{p_1p_1} \to \frac{S_{\overline{pp}}(x_0,\theta_0,f)}{d_0\alpha_0} \times d(\cdots x_1,\theta_1\cdots)\alpha(\cdots\theta_1\cdots),$$
$$S_{p_3p_3} \to \frac{S_{\overline{pp}}(x_0,\theta_0,f)}{d_0\alpha_0} \times d(\cdots x_3,\theta_3\cdots)\alpha(\cdots\theta_3\cdots), \quad \Psi_{p_1\hat{p}_2} \to \beta(\cdots,\theta_1,\theta_2\cdots),$$
$$\Psi_{\hat{p}_2p_3} \to \gamma(\cdots|x_2-x_3|,\theta_3\cdots)\exp[-\mathrm{i}2\pi f(x_3-x_2)/\bar{U}_c(\theta_3)]. \tag{D.5}$$

D.2. Force-per-unit-length CSDs

By analogy with the preceding, the CSD between two oblique forces per unit length, $f_1(x,t)$ and $f_3(x',t)$, can be written in terms of CSDs involving an intermediary force per unit length, $f_2(x,t)$, as

$$S_{f_1f_3}(x,x',f) = [S_{f_1f_1}(x,x,f)S_{f_3f_3}(x',x',f)]^{1/2}\Psi_{f_1\hat{f}_2}(x,x,f) \times \Psi_{\hat{f}_2f_3}(x,x',f), \tag{D.6a}$$

where

$$\Psi_{f_1\hat{f}_2}(x,x,f) = \frac{S_{f_1f_2}(x,x,f)}{[S_{f_1f_1}(x,x,f)S_{\hat{f}_2\hat{f}_2}(x,x,f)]^{1/2}}, \tag{D.6b}$$

$$\Psi_{\hat{f}_2f_3}(x,x',f) = \frac{S_{f_2f_3}(x,x',f)}{[S_{\hat{f}_2\hat{f}_2}(x,x,f)S_{f_3f_3}(x',x',f)]^{1/2}}, \tag{D.6c}$$

and $\hat{f}_2(x,t)$ is that portion of $f_2(x,t)$ that is correlated with both $f_1(x,t)$ and $f_3(x',t)$ (see Fig. 13). As before, the above are exact relations. From Eq. (18), we obtain

$$S_{f_if_i}(x,x,f) = \frac{D^2}{4}\frac{S_{\overline{pp}}(x_0,\theta_0,f)}{d_0\alpha_0}K_{ii,\theta}(\cdots), \quad i = 1,2.3. \tag{D.7}$$

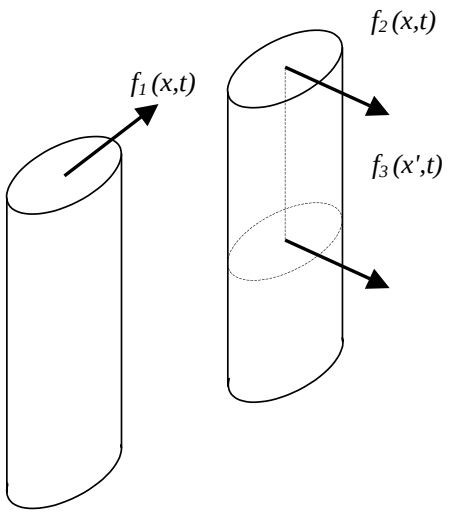

Fig. 13. Diagram used to obtain the CSD of the forces at two arbitrary points on two adjacent cylinders.

Noting this, along with Eqs. (D.6b), (D.6c), and comparing Eq. (D.6a) to Eq. (18), the following associations can be made (assuming $S_{f_2f_2}(x,x,f)$ approximates $S_{\hat{f}_2\hat{f}_2}(x,x,f)$):

$$S_{f_1f_3}(x,x',f) \to S_{f_if_j}(x,x',f), \tag{D.8a}$$

$$\Psi_{f_1\hat{f}_2}(x,x,f) \to \frac{K_{ij,\theta}(\cdots)}{[K_{ii,\theta}(\cdots)K_{jj,\theta}(\cdots)]^{1/2}}, \tag{D.8b}$$

$$\Psi_{\hat{f}_2f_3}(x,x',f) \to \gamma(\cdots|x-x'|\cdots)\exp[-\mathrm{i}2\pi f(x'-x)/(aU)]. \tag{D.8c}$$

In retrospect then, a manipulation (i.e., normalization) of the form of relation (D.8b) would have simplified our expression for the inter-cylinder lateral spectral density factors given by Eq. (23a) in the main text, by factoring out all PSD influences from $K_{ij,\theta}$; but this is now moot.

References

[1] M.P. Païdoussis, Ll.R. Curling, An analytical model for vibration of clusters of flexible cylinders in turbulent axial flow, Journal of Sound and Vibration 98 (1985) 493–517.

[2] Ll.R. Curling, J.O. Gagnon, in: M.P. Paidoussis, M.K. Au Yang (Eds.), A theoretical model for vibration analysis of cylinders in axial flow, Proceedings of ASME Symposium on Flow-Induced Vibrations, Vol. 4: Vibration Induced by Axial and Annular Flows, 1984.

[3] Ll.R. Curling, M.P. Païdoussis, Measurements and characterization of wall pressure fluctuations on cylinders in a bundle in turbulent axial flow. Part 1: spectral characteristics, Journal of Sound and Vibration 157 (1992) 405–433.

[4] M.P. Païdoussis, Dynamics of cylindrical structures subjected to axial flow, Journal of Sound and Vibration 29 (1973) 365–385.

[5] M.P. Païdoussis, The dynamical behaviour of cylindrical structures in axial flow, Nuclear Science and Engineering 1 (1974) 83–106.

[6] Ll.R. Curling, M.P. Païdoussis, Measurements and characterization of wall pressure fluctuations on cylinders in a bundle in turbulent axial flow. Part 2: temporal characteristics, Journal of Sound and Vibration 157 (1992) 435–449.

[7] J.R. Reavis, WVI-Westinghouse vibration correlation for maximum fuel-element displacement in parallel turbulent flow, Transactions of the American Nuclear Society 10 (1967) 369–370.

[8] D.J. Gorman, An analytical and experimental investigation of vibration of cylindrical reactor fuel elements in two-phase parallel flow, Nuclear Science and Engineering 44 (1971) 277–290.

[9] W.T. Thomson, Theory of Vibration with Applications, Prentice-Hall, Englewood Cliffs, NJ, 1981.

[10] Ll.R. Curling, Theory of Vibration of Clusters of Cylinders in Axial Flow, M.Eng. Thesis, Department of Mechanical Engineering, McGill University, Montreal, Quebec, Canada, 1982.

[11] M.P. Païdoussis, S. Suss, Stability of a cluster of flexible cylinders in bounded axial flow, Journal of Applied Mechanics 44 (1977) 401–408.

[12] M.P. Païdoussis, The dynamics of clusters of flexible cylinders in axial flow: Theory and experiments, Journal of Sound and Vibration 65 (1979) 391–417.

[13] M.P. Païdoussis, J.O. Gagnon, Experiments on vibration of clusters of cylinders in axial flow: modal and spectral characteristics, Journal of Sound and Vibration 96 (1984) 341–352.

[14] J.O. GAGNON, Fluid Coupling and Response Characteristics of Cylinder Clusters in Axial Flow, Ph.D. Thesis, Department of Mechanical Engineering, McGill University, Montreal, Quebec, Canada, 1989.

[15] M.P. Païdoussis, Ll.R. Curling, J.O. Gagnon, Experiments on fluidelastic instability of cylinder clusters in axial flow, American Society of Mechanical Engineers Journal of Fluids Engineering 104 (1982) 342–349.

[16] J.O. Gagnon, M.P. Païdoussis, Fluid coupling characteristics and vibration of cylinder clusters in axial flow. Parts 1 and 2, Journal of Fluids and Structures 8 (1994) 257–291.

[17] E. Ohlmer, Experimental investigation of an analytical model for parallel flow induced vibrations of rod structures, in: Symposium on Vibration Problems in Industry, Keswick, UK, Session 5, 1973.
[18] H.P. Bakewell Jr., G.F. Carey, J.J. Libuha, H.H. Schloemer, W.A. Von Winkle, Wall pressure correlations in turbulent pipe flow, U.S. Navy Underwater Sound Laboratory Report No. 559, 1962.
[19] H.P. Bakewell Jr., Narrow-band investigations of the longitudinal space-time correlation function in turbulent airflow, Journal of the Acoustical Society of America 36 (1964) 146–148.
[20] J.M. Clinch, Measurements of the wall pressure field at the surface of a smooth-walled pipe containing turbulent water flow, Journal of Sound and Vibration 9 (1969) 398–419.
[21] W.H. Lin, M.W. Wambsganss, J.A. Jendrzejczyk, Wall pressure fluctuations within a seven-rod array, GEAP Report 24375, General Electric Co., Nuclear Engineering Division, San José, California, 1981.
[22] T.M. Mulcahy, M.W. Wambsganss, W.H. Lin, T.T. Yeh, W.P. Lawrence, Measurements of wall pressure fluctuations on a cylinder in annular water flow with upstream disturbances, Part 1: no flow spoilers, GEAP-24310 General Electric Co., Nuclear Engineering Division, San José, CA, 1981.
[23] W.H. Lin, M.W. Wambsganss, Analytical modeling of the buffeting of a rod in axial flow, GEAP Report 24383, General Electric Co., Nuclear Engineering Division, San José, CA, 1981.
[24] W.H. Lin, Buffeting of a slender circular beam in axial turbulent flows, American Institute Aeronautics and Astronautics 22 (1984) 690–695.
[25] E. Ohlmer, S. Russo, R. Schwemmle, Investigation of an analytical model for parallel flow induced rod vibrations, Nuclear Engineering and Design 22 (1972) 272–289.
[26] Ll.R. Curling, Measurements of Wall Pressure Fluctuations on Cylinders in a Bundle in Turbulent Axial Flow, Ph.D. Thesis, Department of Mechanical Engineering, McGill University, Montreal, Quebec, Canada, 1990.
[27] S.S. Chen, M.W. Wambsganss, Parallel-flow-induced vibration of fuel rods, Nuclear Engineering and Design 18 (1972) 253–278.
[28] D.J. Gorman, The role of turbulence in the vibration of reactor fuel elements in liquid flow, Atomic Energy of Canada Ltd, Report 3371, 1969.
[29] W.W. Willmarth, R.E. Winkel, L.K. Sharma, T.J. Bogar, Axially symmetric turbulent boundary layers on cylinders: mean velocity profiles and wall pressure fluctuations, Journal of Fluid Mechanics 76 (1976) 35–64.
[30] W.W. Willmarth, C.E. Wooldridge, Measurements of the fluctuating pressure at the wall beneath a thick turbulent boundary layer, Journal of Fluid Mechanics 14 (1962) 187–210.
[31] M.K. Bull, Wall-pressure fluctuations, associated with subsonic turbulent boundary layer flow, Journal of Fluid Mechanics 28 (1967) 719–754.
[32] G.M. Corcos, Resolution of pressure in turbulence, Journal of the Acoustical Society of America 35 (1963) 192–199.
[33] H.G. Nepomuceno, R.M. Lueptow, Pressure and shear stress measurements at the wall in a turbulent boundary layer on a cylinder, Physics of Fluids 9 (1997) 2732–2739.